Materials Advances

ROYAL SOCIETY OF CHEMISTRY

REVIEW

View Article Online
View Journal | View Issue

Cite this: *Mater. Adv.*, 2022, 3, 5645

Chitosan- or glycidyl methacrylate-based adsorbents for the removal of dyes from aqueous solutions: a review

Raed A. Mashabi,[a] Ziya A. Khan*[a] and Khalid Z. Elwakeel *[ab]

Dyes have been found in industrial effluent, highlighting the need for effective treatment. Different processes like filtration, flocculation, and adsorption are low-cost, and efficient methods used for the removal of organic pollutants from wastewater (WW). The utilization of natural and synthetic materials for the above-mentioned processes has recently received a lot of attention. Based on the literature, the most promising sorbents are those derived from chitosan (CS) or glycidyl methacrylate (GMA) due to their various properties: availability, stability, sorption capacity, and durability. This overview presents studies involving the use of CS or GMA as dye adsorbents and their modifications using different functional materials. CS and GMA derivatives have good water-purification properties, and they can be utilized to clean WW effectively. This Review highlights the use of CS or GMA in WW treatment from organic dyes. To understand how CS and GMA may remove organic dyes from WW, thorough knowledge of their adsorption capabilities is required. For example, the adsorption capacity of the carboxymethylated CS-conjugated magnetic nano-adsorbent for Acid Orange 12 dye and GMA-substituted dextran with acrylic acid for methylene blue reached 1883 and 1994 mg g^{-1}, respectively. The Langmuir isotherm model and the pseudo-second-order kinetic model were the most applicable for describing dye adsorption. Furthermore, recent breakthroughs in various CS and GMA composites, as well as diverse ways to remove organic dyes from WW, are discussed in multiple instances to offer a framework for future research. The GMA/CS hybrid material is recommended for future investigations. This could be useful for creating more effective contaminant-removal methods, bridging the gap between laboratory results and industrial applications.

Received 20th March 2022,
Accepted 7th June 2022

DOI: 10.1039/d2ma00320a

rsc.li/materials-advances

1. Introduction

Water is an important source of life on Earth. Humanity has faced a global problem in the last few years, which is the shortage of fresh water. Furthermore, it is critical to preserve the ecosystem. It is becoming highly contaminated as a result of continuous industrialization, the discharge of unwanted materials, and everyday human activities. Water contamination is now regarded as a global issue that is growing rapidly.[1] Releasing WW into receiving waterways causes major environmental issues because it contains various organic and inorganic pollutants. Wastewater produced by many industries includes a large number of organic dyes.[2] Pollutants in water bodies degrade the water quality and make it unfit for use.[3] Wastewater that is sometimes known as sewage is the water that is discharged after it has been used by humans.[4] Untreated industrial effluents, farming runoff – including pesticides and fertilizers – medical waste, and home waste discharged into bodies of water are considered as waste polluted water.[5] Effluents of the textile, food, printing, and petroleum sectors contain a variety of organic chemicals, such as dioxins, dibenzofurans, chlorophenols, polychlorinated biphenyls (PCBs), dyes, arsenate, chromate, fluoride, nitrate, and phosphates, and are examples of contaminants.[6] Dyes are recognized as the most hazardous pollutants since they are mutagenic, immunogenic, carcinogenic, and teratogenic.[7] To prevent and minimize water pollution, a range of treatment systems is available, each with varying degrees of effectiveness.[8] Polymers are macromolecules, which are widely distributed in nature and perform several functions in everyday life. Polymers can be divided into two main categories, *e.g.*, (I) bio-based polymers such as chitin,[9] CS,[10] silk fibroin,[11] keratin,[12] starch,[13] *etc.*, and (II) synthetic polymers such as polyethylene,[14] polyethylene terephthalate,[15] polystyrene,[16] and GMA,[17] *etc.* Bio-based polymers have a non-toxic, biodegradable, economical, and environmentally

University of Jeddah, College of Science, Department of Chemistry, Jeddah, Saudi Arabia
[b] *Environmental Chemistry Division, Environmental Science Department, Faculty of Science, Port Said University, Port Said, Egypt.*
E-mail: khalid_elwakeel@sci.psu.edu.eg

friendly nature.[10] Chitin and CS are the most abundant natural polymers on Earth and are important biomass resources that are produced in plants and lower animals, respectively.[18] Chitin is used as raw a material for the production of CS *via* deacetylation.[19] The major steps involved in this conversion are demineralization, deproteinization, and decolorization.[20] Chitosan is a cationic, bioactive, natural polysaccharide formed by glucosamine and *N*-acetylglucosamine subunits attached *via* β-(1–4) linkages. Chitosan is predominantly categorized using FT-IR spectroscopy to determine the rate of deacetylation.[19] Identification of the molecular weight is an essential step for understanding the potential applications of polymers, especially in biological systems. Several factors, *i.e.*, the degree of deacetylation, molecular weight, ionization, and pH, affect the viscosity of CS. The viscosity of the CS solution generally decreases as the temperature is increased.[21] Chitosan is insoluble in water and other organic solvents but can be dissolved in certain organic acids (*i.e.*, acetic acid and formic acid).[22] Chitosan, due to its unique physicochemical properties, has been applied for various functional biomedical and industrial biotechnological applications.[23–25]

Modern research has enabled the development of CS bio-based and hybrid materials for potential applications in antimicrobial packaging, corrosion protection, and the removal of organic dyes.[26] In this regard, CS has been blended with numerous other polymers *e.g.*, poly(methyl methacrylate), polycarbonate, polyaniline, polysulfide, GMA, and polystyrene.[27] Composites of CS exhibit improved material properties, *e.g.*, morphology, surface area, electrical conductivity, mechanical strength, photoluminescence, and bioactive properties, that enable their use in various technical fields such as membrane technology, biosensing, antimicrobial, biomedical materials, packaging, and textiles.[28]

On the other hand, GMA is an attractive vinyl monomer because of its low toxicity, lower cost compared with other acrylic monomers, its versatile properties, and in particular due to the presence of the epoxy group in the molecule,[29] which makes it very reactive for chemical modification or for reacting with other materials. These polymers are potent sorbents for various transition metals.[14,30] Various studies on metal sorption for chitosan-based materials have pointed out limitations in uptake kinetics due to its resistance to intraparticle diffusion (which may be explained by the residual crystallinity of the biopolymer and by poor porous and surface properties). This drawback was partially solved by changing the conditioning of the biopolymer (the manufacturing of gel beads, membranes, and so on). Another possibility consists of the preparation of a chitosan/GMA hybrid material, which is expected to enhance the physical and chemical properties of the hybrid material; in addition, the reactivity of the hybrid sorbent can be improved by grafting new functional groups such as different amines on the epoxy group of GMA.

This article aims to review the use and future outlook for CS or GMA-based sorbents as a cost-effective and environmentally friendly way to remove organic dyes from WW. The sorbents can be modified using many physical and chemical methods to increase the surface area, functional groups, and sorption active sites. There are several mechanisms of adsorption for the removal of organic dyes, mostly involving the contact of electrostatics, ion exchange, and complexation. Due to the great progress in the creation of various sorbents, there are still several issues connected with these materials, such as pH stability, sorption capacity and durability, that need to be addressed. This Review will focus on the potential applications of CS, GMA, and the chitosan/GMA hybrid material as potential tools for the adsorption of anionic dyes from water. This Review summarizes recent studies that address the removal of organic dyes using CS and GMA adsorbents. We then examine various CS and GMA-based adsorbents that are capable of removing organic dyes from WW and describe their characteristics, and we discuss the adsorption mechanisms involved that might be relevant to future projects for the treatment of WW.

2. Dyes

Dyes are color-inducing chemical substances that adhere to fabrics or surface shells. Because dyes are water-soluble and produce exceptionally bright colors in water with acidic qualities, depolarization of WW from the textile and other industries is a serious concern for environmental management. Synthetic dyes may be included in WW effluents, which pose a risk to the environment. Different separation strategies have been explored in the removal of dyes from aqueous solutions due to environmental and health problems related to WW effluents. Physical, chemical, and biological procedures are used to remove dyes from WW.[31]

2.1. Sources of dyes

Dyes are primarily generated from natural sources such as plants, insects, animals, and minerals that have not been chemically treated. Indigo and saffron are plant-based dyes, cochineal beetles and lac scale insects produce dyes from insects, animal-based dyes are obtained from molluscs or shellfish, and examples of mineral dyes are ferrous sulfate and ochre. Anionic, cationic, and non-ionic dyes are the most common classifications. Table 1 reports some selected examples of dyes and their uses. These dyes are always found in industrial waste and, as a result, are dumped into bodies of water. Various industries, such as textile, paper, food coloring, cosmetics, leather, pharmaceutical, dyeing, printing, and carpet industries employ dyes to color their products, and then discharge them into WW. Out of all the industries that use dyes, the textile industry is ranked top in the use of dyes for fiber coloration. It is estimated that the textile and manufacturing industries use more than 10 000 commercially accessible (global) dyes, with the textile industry consuming more than 1000 tons per year, with about 10–15% of these dyes being released into waste streams as effluents during dyeing processes.[31] Adding even a small amount of dye to an aquatic system disrupts the delicate balance of the system by lowering the gas solubility, water transparency, and photosynthetic activity, all of which are required for aquatic plants and wildlife to exist.[32]

Table 1 Some examples of dyes and their uses

Nature	Example	Structure	Use	Ref.
	Methyl Orange (MO)	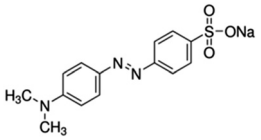	Indicator	33, 34
Anionic	Remazol black B (reactive black 5)	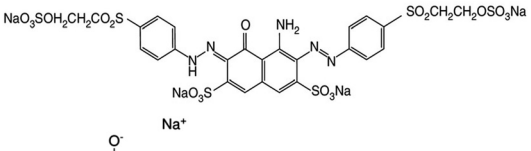	On wool, cotton, and viscose.	35
	Coomassie brilliant blue (CBB)	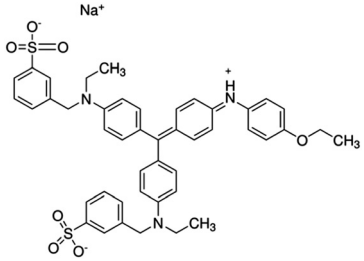	Protein determination and surface-enhanced Raman spectroscopy	36
	Brilliant red 3B-A (BR3B-A)	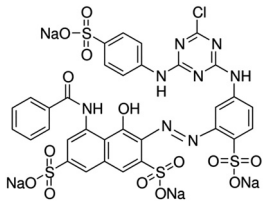	In the industrial field, it is utilized as an azo dye.	37
Cationic	Vat dye	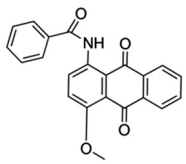	Used for cotton dyeing	38

Table 2 The benefits and drawbacks of various dyes removal technologies

Technique	Advantages	Disadvantages	Ref.
Adsorption	Low-cost, recyclable, dye, metal, and microbial removal	pH-dependent, formation and losses during regeneration	39
Coagulation	Simple to handle, cost-effective, and easy to run.	Causes waste sludge in higher quantities. Acid-based dyes are less efficient.	40
Electrochemical	The process is efficient, simple to run, and produces no sludge. Effective at removing metal and colors.	It is costly, requires the use of electrical equipment, an inefficient dye-removal method.	41
Biological method	Environmentally benign, simple to operate, low-cost,	Not efficient in the regeneration process	42
Membrane filtration	Purification of all micro-pollutants, autonomous operation, rapid removal of dyes	High cost, management and fouling issues, regeneration	43

3. Dyes removal technologies

The removal of dye molecules from water sources has become a serious environmental problem as well as a significant task in recent years. Various dye-removal procedures have been established in numerous research publications (Table 2), all of which claim to be successful. Although there are numerous existing tried-and-tested methods to accomplish dye removal, most of them have a common disadvantage, which is the generation of secondary pollution to the environment. A good dye-removal process should be able to remove large amounts of dye from WW in a short amount of time without causing any secondary pollution. Adsorption is a high-quality treatment process for removing dissolved dyes from industrial WW.

4. Biopolymers

Biopolymers are a new type of green material with a great performance and low weight. Biopolymers, often known as biodegradable polymers, are polymeric materials that degrade in part through the metabolism of naturally existing organisms.

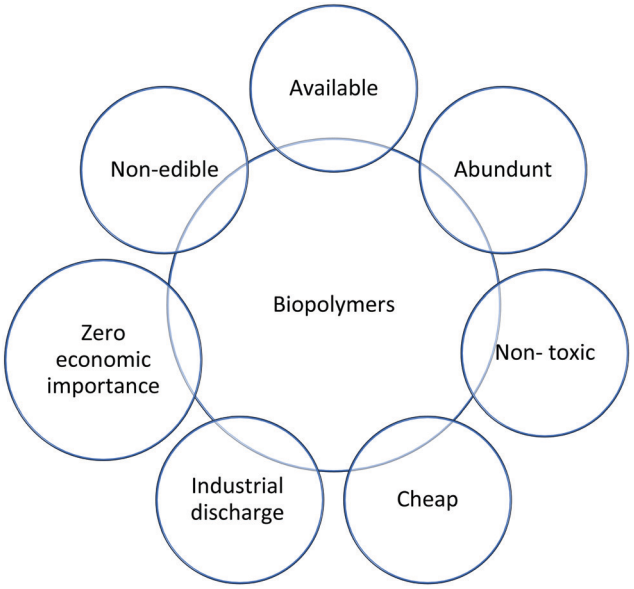

Fig. 1 Advantages of biopolymers.

Under appropriate conditions of moisture, temperature, and oxygen availability, biodegradation leads to fragmentation or disintegration with no toxic or environmentally harmful residue. The advantages of biopolymers are shown in Fig. 1. Biopolymers can be classified into several groups based on the raw ingredients used and the manufacturing procedures used, as depicted in Table 3.[44,45]

5. Chitosan

Chitosan is a polysaccharide derived from chitin, which is the second most abundant biopolymer in nature after cellulose.[46] Chitosan (poly-β-(1,4)-2-amino-2-deoxy-D-glucose) is a non-hazardous and potent adsorbent that is commonly employed in the adsorption process among the different solid, low-cost adsorbents available for pollutant removal.[47] According to its structural features (Fig. 2), it has a high adsorption capacity for dye molecules due to the huge number of active hydroxyl (–OH) and amine ($–NH_2$) groups in the macromolecular chain.[48] Chitosan offers several advantages, including a macromolecular structure, non-toxicity, biocompatibility, low cost, broad applicability, high porosity, low density, renewability, biodegradability, and high adsorption potential. The use of CS for pollutant removal from WW is based on three factors: (I) CS-based polymers are

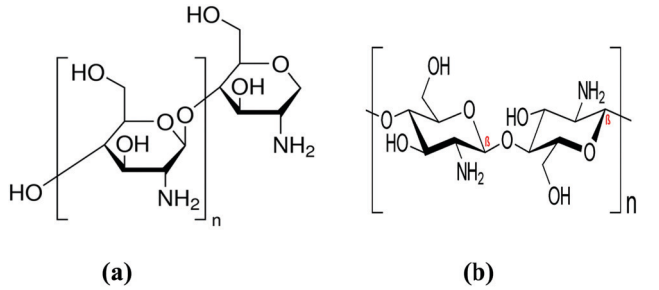

Fig. 2 (a) Chitosan; and (b) β-(1–4) chitosan structures.

inexpensive materials derived from natural resources, and their use as a bio-sorbent is particularly economically efficient; (II) high adsorption capabilities and increased adsorption rates have been discovered; and (III) the simplicity with which CS can be modified and combined.[49] The sorption capacity of CS-based sorbents is high for many of the most prevalent pollutants encountered in effluents from the dyeing industry, and it can have a sorption capacity that is many times greater than commercial adsorbents. Chitosan is a positively charged surface that interacts electrostatically with dye anions, which considerably increases its dye sorption.[50] The grafting (inserting functional groups) or crosslinking processes (uniting the macromolecular chains) of the chitosan molecule result in the production of chitosan derivatives with improved characteristics (adsorption capacity and resistance improvements under extreme medium conditions, respectively).[47] Unmodified and modified CS, as well as its numerous derivatives, are used in dye adsorption, air pollution, heavy-metal adsorption, biomedical, and other applications.[3] Chitosan also has some disadvantages, such as low acidic medium stability, and low cationic dye adsorption effectiveness, which need to be addressed to meet the requirements of treating WW in practical applications.[48]

5.1. Grafted chitosan

PAMAM-grafted chitosan as a biocompatible adsorbent was synthesized by Banisheykholeslami *et al.* in 2021,[51] *via* the Michael addition of methyl acrylate followed by amidation of ethylene–diamine on the CS backbone. Then, the adsorption capacity of bio-adsorbents was assessed using two anionic dyes. The adsorption experiments were carried out using a batch adsorption system. The influence of various operational variables such as different PAMAM generations, pH, adsorbent dosage, contact time, initial dye concentration, and temperature on the maximum adsorption capacity (q_m) was investigated.

Table 3 Biopolymer classification

	Class	Source	Examples
Biopolymers	Polysaccharides	Plant	Starch, cellulose, pectin, alginate, and gum
		Animal	Chitin, chitosan, glycogen, and alginate
		Microorganisms	Cellulose, dextran, pullulan, and gellan gum
	Proteins	Plant	Soy proteins, zein protein, and gluten
		Animal	Casein, collagen, whey, and fish protein
		Microorganisms	Cyanophycin, poly-γ-glutamate, and polyphosphate
	Polyesters	Microorganisms	Poly(hydroxy alkanoates)

The adsorbent consisting of second-generation PAMAM (CS–PAMAM G2) demonstrated a high removal efficiency for both dyes. The maximum adsorption capacity of CS–PAMAM G2 for Congo red (CR) under certain operational conditions was 559.3 mg g^{-1}, while the maximum adsorption capacity for amido black 10B (AB10B) under certain operational conditions was 489.8 mg g^{-1}, which revealed the endothermic and exothermic nature of the adsorption process for CR and AB10B, respectively. These results were then confirmed satisfactorily using thermodynamics studies. Also, kinetic studies showed that the dye-adsorption process followed a pseudo-second-order (PSO) kinetic model. Moreover, among the various applied isotherms, the experimental data were well-fitted by the Sips model. Consequently, CS–PAMAM G2 showed superior potential for the removal of dyes from the aqueous phase.

Novel, eco-friendly CS–genipin–cellulose hydrogel beads grafted with dimethyl-diallyl-ammonium chloride (CS–G–Cell-*g*-DMDAAC), were prepared here[42] as selective adsorbents for anionic dyes. The physical and chemical structural changes of the prepared hydrogel were evaluated using FT-IR, XRD, SEM, and TG-DSC analysis. Results showed CS–G–Cell-*g*-DMDAAC efficiently and selectively adsorbed anionic dyes reactive red 195 (RR195) and methyl orange (MO) from a mixture of dye solutions. The CS-based hydrogels were endowed with the advantages of acid insolubility and good adsorption. The RR195 and MO adsorption processes were described better with a PSO kinetic model and a Langmuir isotherm model with a maximum adsorption capacity of 1333.52 and 190.48 mg g^{-1}, respectively, indicating that monolayer chemisorption controlled the sorption process. The hydrogels are promising for potential applications in WW treatment.

According to Ahmad *et al.*[52] the polymerization of pyrrole with various weight fractions of ZnO (Z) yielded a bio-nanocomposite matrix of polypyrrole (Pp)-grafted Z–CS (Pp–Z–CS). The photocatalytic, antibacterial, and cytotoxic capabilities of the composite emerged from combining Z nanoparticles with Pp. XRD, FT-IR, TGA, and DTA were used to characterize the product. SEM and TEM were used to determine the surface morphology and particle size, respectively. The photocatalytic activity of the composite material was tested by monitoring the degradation of reactive orange 16 (RO16), Coomassie brilliant blue R-250 (CBBR-250), and methylene blue (MB) dyes, and the composite was found to be an effective catalyst in the presence of a UV light source. The surface morphology of the as-prepared bio-nanocomposites was studied *via* SEM, whereas the particle size and elemental composition of the as-synthesized bio-nanocomposites were studied *via* TEM and EDX analysis, respectively. As shown in Fig. 3a, the presence of Z nanoparticles doped on Pp can be observed in which Z nanorods are scattered over the surface of the Pp. The matrices of Z, CS, and Pp are mixed irregularly, as shown in Fig. 3b. The microscopic particles of Z are seen to be adsorbed and dispersed on the surface of Pp irregularly. The polymer matrices of the nanocomposites, Pp and CS are mixed, as shown in Fig. 3c. TEM micrographs of the matrix show the particle size of the nanocomposites, which is in the range of 10–100 nm. In Fig. 4a, the nanorods of Z are shown

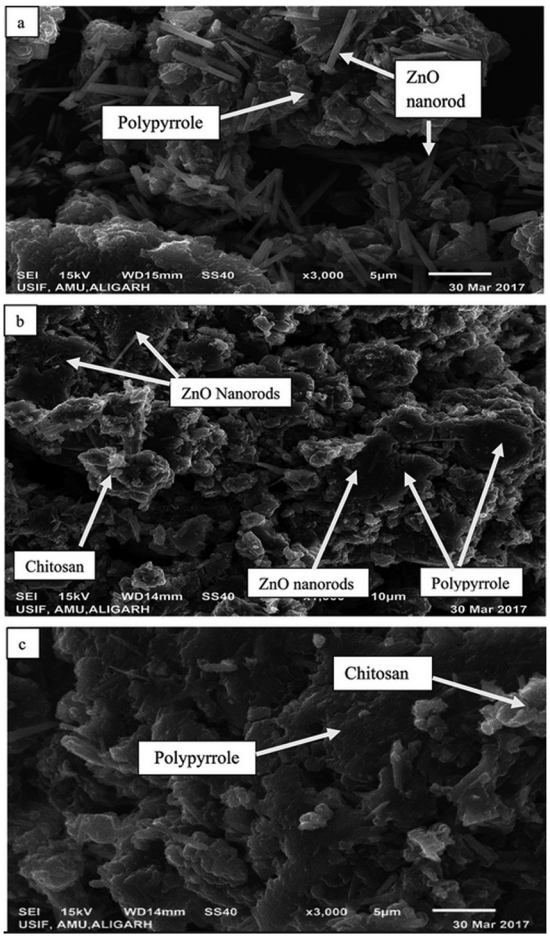

Fig. 3 SEM images of the as-prepared nanoparticles and nanocomposites: (a) Pp–Z, (b) Pp–CS–Z, and (c) Pp–CS.[52]

to be uniformly mixed with Pp. Fig. 4b shows the TEM images of pure Pp, and two different phases of Pp and CS can easily be seen in Fig. 4c. The Z nanorods are easily dispersed over the Pp surface due to their porous structure. The grain size of Pp increased upon the incorporation of Z as compared with pure Pp and CS, as shown in Fig. 4d.[52]

In membrane preparation and adsorption efficiency, the electrospun polyacrylonitrile (PAN) nanofiber membrane was functionalized with CS and proteins for use in the treatment of dye-containing WW.[53] The PAN nanofiber membrane was subjected to alkaline hydrolysis, before being grafted with CS and subsequently the proteins from chicken egg white. The resultant nanofiber membrane was comprehensively characterized using TGA, FT-IR spectroscopy, and SEM. The efficiency of the membrane in removing toluidine blue O (TBO) and acid orange 7 (AO7) in an aqueous solution was evaluated. Based on the performance of the model fitting, Langmuir and PSO kinetic models could be used to describe the performance of the membrane in the removal of TBO (pH 10), and AO7 (pH 2) from the dye solutions. The adsorbed TBO and AO7 dyes can be completely desorbed using an elution solution made of 50% (v/v) ethanol and 1 M sodium chloride. After five consecutive

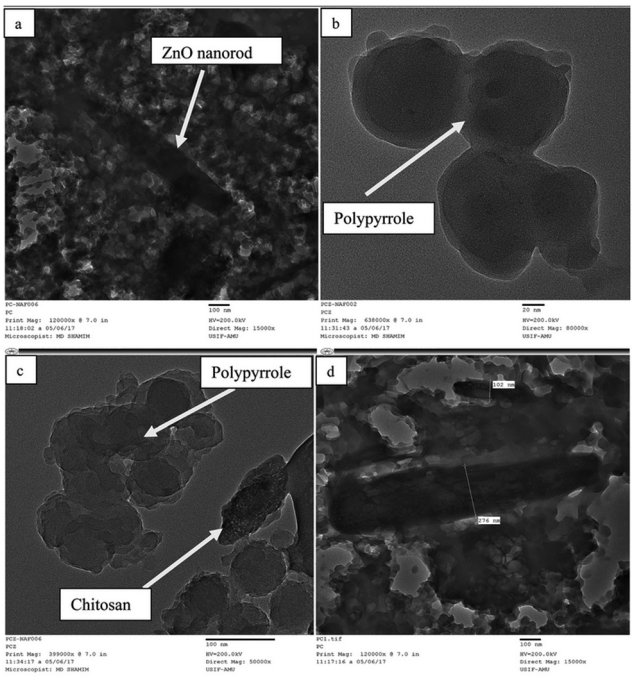

Fig. 4 TEM micrographs of the as-prepared nanoparticles and nanocomposites: (a) Pp–Z, (b) Pp, (c) Pp–CS, and (d) Pp–CS–Z.[52]

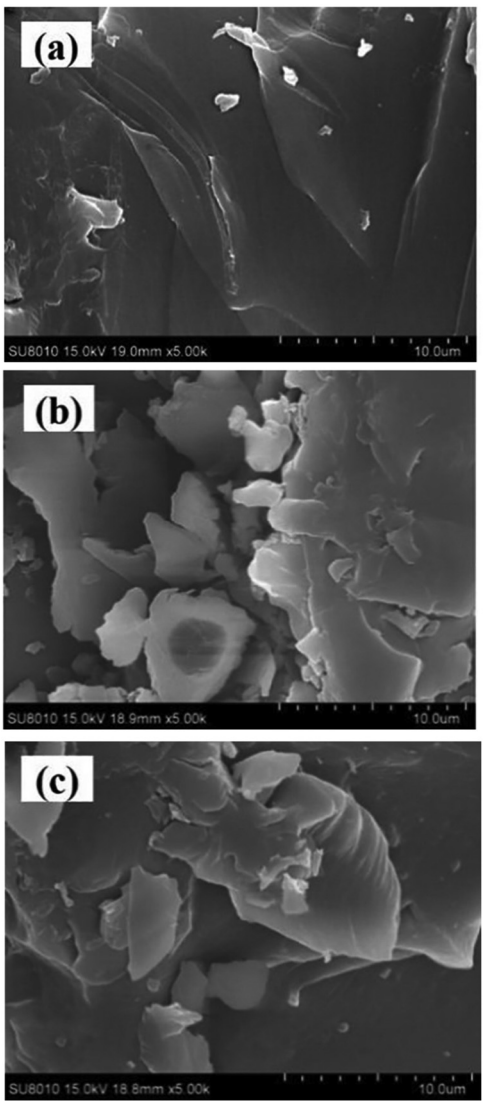

Fig. 5 Morphology of (a) CS, (b) PAA–PAM–CS, and (c) g-CS.[54] Reproduced from ref. 54, with permission from Elsevier, 2020.

adsorption–desorption cycles, the efficiency of dye removal by the membrane was maintained above 97%.[53]

Cui *et al.*[54] obtained a grafted-crosslinked CS for the treatment WW containing organic dyes by inserting poly(acrylic acid) (PAA) and polyacrylamide (PAM) altogether on the CS chain to give PAA–PAM–CS, then coordinated PAA–PAM–CS with Fe(III) to obtain Fe–PAA–PAM–CS (g-CS). SEM, EDS, XRD, TGA, FT-IR, and nitrogen adsorption and desorption studies were used to characterize the two adsorbents, PAA–PAM–CS and g-CS, completely. In an adsorption experiment, PAA–PAM–CS showed excellent adsorption of methylene blue (MB), while g-CS showed the effective removal of reactive brilliant red (RBR). In the adsorption process, the effects of the solution pH, salt content, and temperature were studied. At pH 12, PAA–PAM–CS had a maximum adsorption capacity of 79.09 mg g^{-1} for MB, and g-CS had a maximum absorbance of 918.53 mg g^{-1} for RBR. According to the findings, both adsorption processes involved monolayer adsorption and corresponded to the PSO model and the Langmuir isotherm model. This study revealed a simple and precise approach for removing dyes from WW. Fig. 5(a)–(c) shows the morphology of CS, PAA–PAM–CS, and g-CS, respectively. It can be seen that all three materials are irregular in shape with relatively flat surfaces.[54]

In another study[55] millimeter-scale hollow spheres made from CS, dimethyl diallyl ammonium chloride (DMDAAC), and carboxymethyl cellulose (CM-Cell), were prepared *via* a simple one-pot process of physical stirring and chemical grafting to effectively and selectively remove organic dyes from WW. By introducing the positively charged monomer of DMDAAC, the cationic hollow spheres showed an excellent adsorption capacity toward the organic dyes. The adsorption kinetics and isotherm data were fitted well with PSO and Langmuir models, respectively. The selective removal ratio of reactive black-5 (RB5) was as high as 99.1% from an RB5–Yellow 7 GL mixed solution. The novel hollow spheres not only open a new avenue for the preparation of large-sized hollow spheres but also has broad applications for selective pollutant removal.[55]

Feng *et al.*[56] focused on the preparation and synthesis of flocculants of CS *via* facile grafting and modification to enhance and enlarge its original functions; also characterized CS to have many functional amino and hydroxyl groups. A new type of graft-modified flocculant CS-*g*-AA and its combination with kaolin was developed for the treatment of acid blue 83 (AB83). The composite was prepared *via* the ultrasonic initiation of acrylamide (AM), 3-acrylamide propyltrimethylammonium chloride (APTMAC), and CS. The factors affecting the CS-*g*-AA molecular weight and the CS graft ratio were examined to gain a better understanding and comprehension of the

ultrasonically initiated polymerization. The structure and morphological characteristics of CS-*g*-AA were investigated and analyzed using FT-IR, SEM, ^{1}H NMR, differential thermal/thermogravimetric (TG-DSC), and XRD, respectively. The results indicated that the CS cyclic structure was broken by ultrasonic initiation, and the grafting occurred at the amino group with the C-2 site of CS. Meanwhile, CS-*g*-AA coupled with kaolin exhibited a superior flocculation performance that was better than the single removal effect, and the optimum removal rate for AB83 reached 91.9%. The flocculation mechanism was discussed and summarized based on the results of zeta potential analysis and FT-IR of the floc particles, and the adsorption ability of the formed kaolin flocs. During AB83 flocculation, CS-*g*-AA adsorption and flocculation contributed much to the removal of AB83. The added kaolin particles played a crucial role in enhancing the AB83 adsorption and flocculation. The kaolin particles and the formed kaolin floc showed an adsorption effect for AB83, and the kaolin particles also worked as a bridge between CS-*g*-AA filled with AB83 moieties to strengthen the flocculation performance.[56]

Lu *et al.*[57] prepared a porous magnetic adsorbent with a sufficiently interconnected pore structure of CS-*g*-poly(2-acrylamide-2-methylpropane sulfonic acid) (CS-*g*-AMS) by grafting AMS onto CS *via* Pickering high internal phase emulsion polymerization, which stabilized with the modified Fe_3O_4 nanoparticles, and was used for removal of the organic dyes methylene blue (MB), brilliant green (BG), and methyl green (MG) from an aqueous solution. The effects of the starting pH, contact time, and the initial concentration on the porous adsorption characteristics were explored. The porous magnetic adsorbent was found to rapidly adsorb MB, BG, and MG with high adsorption capacities across a pH range of 6–12. In 20 minutes, the maximal adsorption capacities of MB, BG, and MG were 1044.56, 1625.94, and 908.01 mg g^{-1}, respectively. After the adsorption of MB, BG, and MG, the adsorbent can be easily recycled from the solution using a magnet and be regenerated for re-use. After five adsorption–desorption cycles, the adsorption capabilities of MB, BG, and MG were 1010.02, 1578.73, and 889.01 mg g^{-1}, respectively. The recyclable adsorbent showed a high adsorption capacity, a rapid adsorption rate, and great re-usability, and could be utilized to remove dye from WW.[57]

In another investigation, Singh *et al.*[58] reported on the peroxydisulfate–ascorbic acid (PDSAA)-initiated synthesis of CS-*g*-poly(methyl methacrylate) (CS-*g*-MMA) and its characterization *via* FT-IR, XRD, and ^{13}C NMR. The copolymer remained water-insoluble even under highly acidic conditions and was evaluated to be an efficient adsorbent for three azo dyes: Procion yellow MX (PY), Remazol brilliant violet (RBV), and reactive blue H5G (RB) over a wide pH range of 4–10, albeit mostly at pH 7. The adsorbent was also found to be significantly more effective than the original CS at cleaning textile-industry WW. At various pH values and initial dye concentrations, adsorption isotherm studies were carried out. The experimental equilibrium data for each adsorbent dye system were successfully fitted to the Langmuir and Freundlich sorption isotherms. At pH 7, the parent CS also showed PSO kinetics. The temperature dependence of dye uptake and the PSO kinetics of the adsorption indicated that chemisorption is the rate-limiting step that controls the process.[58]

Wang *et al.*[59] removed methylene b(MB) from an aqueous solution with CS-*g*-poly(acrylic acid)–attapulgite (CS-*g*-AA–AP) composites as the adsorbent, and carried out some batch adsorption tests. The effects of the AP content, the initial pH value of the dye solution, and the temperature on adsorption were investigated. Results showed that the AP content of the composites had some influence on the adsorption capacity, and introducing a small amount of AP could improve the adsorption capacity of CS-*g*-AA to a certain extent. Results from kinetic experimental data showed that the adsorption rate of MB on CS-*g*-AA and CS-*g*-AA–AP with 30% of AP was fast, and more than 90% of the maximum adsorption capacities for MB were achieved within the initial 15 min. The adsorption behavior of CS-*g*-AA and CS-*g*-AA–AP showed that the adsorption kinetics and isotherms were in good agreement with a PSO equation and the Langmuir equation, and the maximum adsorption capacities reached 1873 and 1848 mg g^{-1} for CS-*g*-AA and CS-*g*-AA–AP, respectively. The discussion results of desorption studies implied that CS-*g*-AA and CS-*g*-AA–AP can be used as promising adsorbents for the removal of MB from WW.[59]

Fang and co-workers[60] prepared a novel calix[4]crown-grafted CS chelating polymer in good yield *via* the Schiff-base condensation of formacyl calix[4]crown with raw CS (C4–C2-*g*-CS). The structure of the prepared polymer was confirmed using elemental analysis, FT-IR, and XRD analysis. Elemental analysis suggests that the grafting degree of the C4–C2 unit was 22% on the amino groups of CS. The morphological characteristics of the prepared polymer were studied using SEM. The polymer surface possessed a loose porous and smooth morphology. The dye-adsorption ability of the prepared polymer for a series of organic dyes, such as orange I (OI), neutral r(NR), Victoria blue B (VBB), and brilliant green (BG) were studied *via* solid–liquid adsorption experiments. The adsorption percentages increased from 45–60% (raw CS for dyes) to 75–90% (polymer C4–C2-*g*-CS for dyes). The highest adsorption percentage reached 89% for VBB. The saturated adsorption capacities for OI, NR, VBB, and BG were as high as 622, 564, 854, and 781 mg g^{-1}, respectively. The adsorption abilities remained stable at 70–90% in the pH range of 5–9. The adsorption ability for OI decreased gradually with the increase of the solution pH. The adsorption percentages were 70–90% after five cycles of adsorption.[60]

Sehil *et al.*[61] developed a new 3D CS-*g*-polyacrylamide (CS-*g*-PAA) hydrogel through radical polymerization using sodium trimetaphosphate (TMP) as a crosslinking agent. Structural confirmation of the synthesized hydrogel was carried out using FT-IR and X-ray diffraction analysis. In addition, the thermal behavior of the above hydrogel was investigated using thermogravimetric analysis and differential thermal analysis. Moreover, the kinetics and swelling behavior of the resulting product were also studied. The hydrogel obtained was used as an adsorbent to remove organic dyes from aqueous solutions. It was found that the hydrogel possessed a high adsorption capacity that reached 872 mg g^{-1} under optimum conditions. Thus, kinetic,

thermodynamic, and adsorption isotherm models were employed to describe the adsorption process of methylene blue (MB) onto the CS-based hydrogel. The results obtained suggested that the adsorption of MB onto the hydrogel is fitted well with the PSO and Freundlich models. According to thermodynamic studies, it was revealed that the adsorption of MB onto the hydrogel was a spontaneous and exothermic process.[61]

5.2. Magnetic chitosan

In their study, Patel and Patel[62] designed the CS-*g*-poly(IA-*co*-DADMAC)–Fe_3O_4 polymer composite hydrogel using an *in situ* ultrasonic wave-assisted polymerization method and applied it for the uptake of methylene blue (MB) and Congo red (CR) dyes from aqueous solutions. The polymer composite hydrogel was characterized *via* FT-IR, XRD, TGA, FE-SEM, BET, and VSM analyses. More interestingly, the dyes can be efficiently adsorbed, and after adsorption they can be conveniently separated from the solution using an external magnet. For dye-adsorption studies, CR and MB were taken as the target pollutant. The adsorption isotherm followed the Freundlich model with adsorption capacities of 862.06 mg g^{-1} and 1111.11 mg g^{-1}, respectively, and the adsorption kinetics were most appropriately explained using the PSO kinetic model. This study will provide a new perspective on the design and fabrication of novel, safe and effective systems for dye removal. The surface morphologies of the polymer composite hydrogel and the dye-adsorbed polymer composite hydrogel were investigated *via* SEM in Fig. 6. It can be seen that the surface morphology of the polymer composite hydrogel is different from that of dye-adsorbed polymer composite hydrogel Fig. 6(a) and (b). The polymer composite hydrogel presents an uneven and rough surface while the surface of the dye-adsorbed polymer composite hydrogel is smoother and homogeneous. After the adsorption of dye molecules, the polymer composite hydrogel exhibits a different morphology compared with before adsorption. The rough, and uneven surface of the polymer composite hydrogel had increased active adsorption sites and provides conditions to attract more target dye pollutants around the adsorption sites, which improved the rate of adsorption and the adsorption capacity.[62]

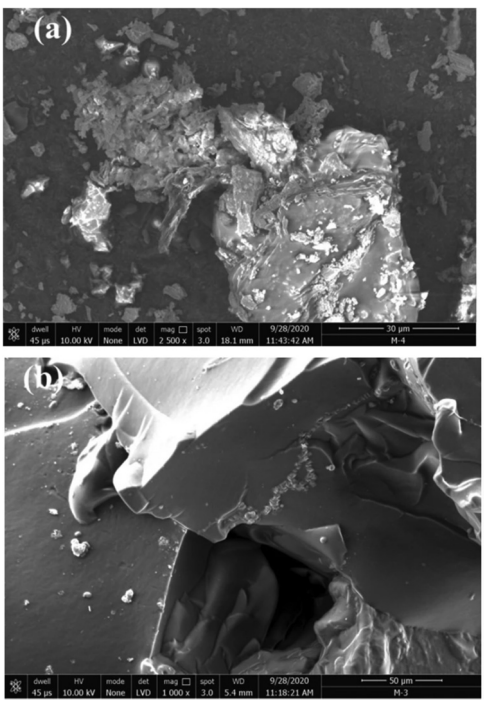

Fig. 6 Typical SEM images of polymer composite hydrogel (a) before dye adsorption, and (b) after dye adsorption.[62] Reproduced from ref. 62, with permission from Springer Nature, 2022.

The economical adsorbent epichlorohydrin-cross-linked CS–magnetic Fe_3O_4-activated carbon nanocomposite, CH-EP@Fe_3O_4/AC, was successfully synthesized for the simultaneous removal of mercury ions and cationic and anionic dyes.[63] The prepared adsorbent was characterized *via* FT-IR, XRD, SEM, TGA, Brunauer–Emmett–Teller (BET) analyses as well as a vibrating sample magnetometer (VSM). According to the results of the BET isotherm, the prepared adsorbent has a specific surface area of 287 m^2 g^{-1}, which offers a relatively high adsorption capacity for the organic dyes. The Box–Behnken design was employed to assist with tuning the optimum adsorption conditions, such as the dosage of adsorbent, solution pH, and contact time. Under the optimized conditions, the kinetics results showed that the adsorption fitted the PSO model well. The Langmuir isotherm fitted well with experimental data of MG and RR120 in single-component solutions, which demonstrated the monolayer process. Also, the experimental data for the adsorption of pollutants in binary and multicomponent solutions exhibited the best fit with the Freundlich model, which shows multilayer adsorption on the surface of the CH-EP@Fe_3O_4/AC adsorbent. The removal efficiency of MG in the solution is about 81% with the maximum adsorption capacity of 146.3 mg g^{-1}, and the removal efficiency and the maximum adsorption capacity of RR120 are 78% and 140.7 mg g^{-1}, respectively. Also, thermodynamic studies demonstrated that the adsorption of pollutants was spontaneous, which was endothermic with an enhancement in entropy. It was observed that the prepared adsorbent was stable after five cycles of adsorption–desorption. Therefore, it was concluded that the prepared nanocomposite is a potential applicant for the adsorption of dyes from mixed aqueous solutions.[63]

Magnetic Fe_3O_4–CS (MFe_3O_4–CS) was successfully prepared *in situ* by Cao *et al.*[64] A simple reduction–precipitation method was used, through the partial reduction of Fe^{3+} with sodium sulfite, precipitation with ammonia at room temperature, and then cross-linking with epoxy chloropropane. The MFe_3O_4–CS was characterized using HR-TEM, BET, XRD, FT-IR, TGA, and VSM. The MFe_3O_4-CS particles were quasi-spherical or ellipsoidal and about 7 nm in average diameter, and exhibited superparamagnetic properties with a saturation magnetization value of 17.1 emu g^{-1}. The adsorption behavior of MFe_3O_4–CS towards reactive brilliant red X-3B (RBR) was investigated, including the pH effect, adsorbent dosage, adsorption equilibrium, and adsorption kinetics. It was found that the adsorption performance of RBR on MFe_3O_4–CS was strongly dependent on both the initial pH and the adsorbent dosage. The adsorption

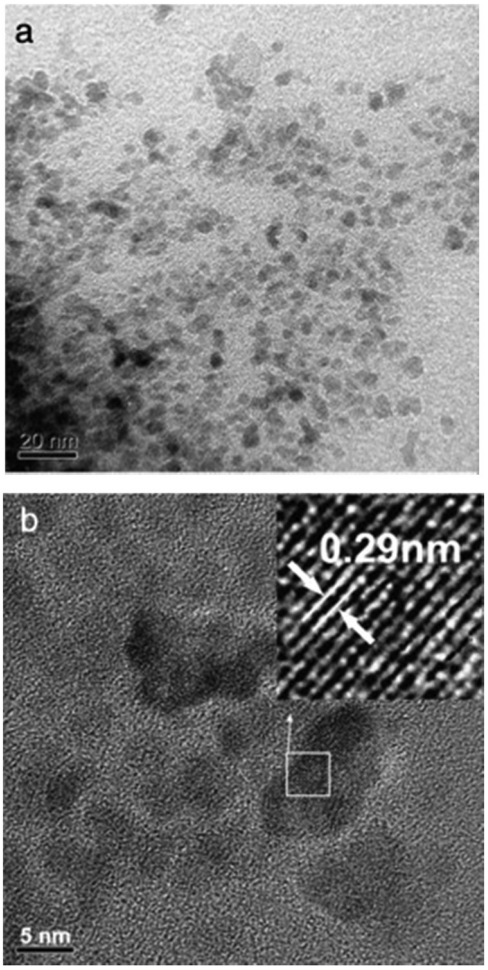

Fig. 7 TEM (a) and HR-TEM (b) images of MFe_3O_4–CS.[64] Reproduced from ref. 64, with permission from Elsevier, 2014.

equilibrium data fitted well with the Langmuir isotherm model and the adsorption process followed the PSO kinetic model. As seen in Fig. 7a and b, the nanoparticles were quasi-spherical or ellipsoidal and the diameter was about 5–8 nm.[64]

In another investigation,[65] magnetic CS biochar was magnetized *via* chemical coprecipitation after loading CS with Schiff base reaction. The prepared magnetic CS biochar was used to remove amaranth dye from solutions. The synthesized magnetic CS biochar was characterized to define its surface morphology and specific elements. The amaranth-dye-adsorption system was optimized by varying the contact time, pH, and initial concentration. The adsorption of magnetic CS biochar on the amaranth dye was measured over a wide pH range. According to zeta potential measurements, the surface of magnetic CS biochar was positively charged in the acidic pH region, which was more conducive to the adsorption of amaranth dye. In addition, the adsorption data were fitted with the pseudo-first-order (PFO) kinetic model and the Langmuir adsorption model and the maximum adsorption capacity reached 404.18 mg g^{-1}. The adsorption efficiency of magnetic CS biochar was still above 95% after three cycles of adsorption–desorption. The removal percentage in a real sample of amaranth dye by the magnetic CS biochar was within 94.5–98.6% and the RSD was within 0.14–1.08%. The magnetic CS biochar adsorbent had the advantages of being easy to prepare, easy to separate from solution after adsorption, has a good adsorption performance for amaranth dye and is an effective potential adsorbent for the removal of organic dyes in WW.[65]

A versatile EDTA and CS bi-functionalized magnetic bamboo biochar adsorbent (ECS–MBB) was synthesized for the co-instantaneous adsorption of methyl orange (MO).[66] In this case, the as-synthesized ECS–MBB composite inherited a favorable MO removal performance from the bamboo biochar (BB) obtained at 700 °C through electrostatic attractions, hydrogen bonding, and π–π interactions, and the binding of cationic metals was enhanced by introducing the amino groups of CS and the carboxyl groups of EDTA. In the unitary system, the removal of MO using three as-prepared adsorbents can be well fitted by the PSO kinetic model and Langmuir isotherm theory. The saturated capture amounts of ECS–MBB at 25 °C are 305.4 mg g^{-1} for MO, which, under the same conditions, are 1.3, 2.6, and 2.5 times those of CS-modified magnetic bamboo biochar (CS–MBB) and 1.9, 6.1, and 5.4 times those of magnetic bamboo biochar (MBB), respectively. Furthermore, ECS–MBB exhibited no significant loss in adsorption efficiency even after eight adsorption–desorption cycles. This study lays the foundation for fabricating the desired integrative biochar adsorbents in the purification of complex organic pollutants from WW.[66]

Elwakeel *et al.*[67] combined CS with GMA and magnetite to produce a novel magnetic macro-reticular hybrid synthetic–natural material (MCS–GMA). The composite sorbent was modified directly with diethylenetriamine to produce MCS–GMA-I and using epichlorohydrin followed by diethylenetriamine to produce MCS–GMA-II. The surface morphologies of MCGMA-I (before and after sorption) and MCGMA-II (before and after sorption) are shown in Fig. 8 and 9, respectively. The SEM micrographs reveal that the surface of both sorbents is porous, which can be clearly seen in the magnified view of the SEM micrographs, and sorption of the dye changed the surface structures of both MC–GMA sorbents. The amino group concentration in the obtained materials was enriched through two different modification routes to generate effective sorbents for Remazol brilliant blue R (RBBR) ions. These materials showed a higher affinity towards the uptake of RBBR ions from aqueous media: the maximum sorption capacity reached 0.153 mmol g^{-1} at pH 2 and 25 °C. The nature of the interaction of RBBR with the sorbents was identified. The uptake kinetics and sorption isotherms were best described by the PSO rate equation and the Langmuir equation, respectively. The distribution coefficient was calculated at different temperatures and the thermodynamic parameters have been calculated. The sorption reaction is endothermic, spontaneous, and increases the entropy of the system. An alkaline solution (0.5 M NaOH) was used for desorbing the RBBR from the loaded sorbents, and a regeneration efficiency as high as 90–99% was obtained.[67]

In 2017, Elwakeel *et al.*[68] prepared magnetic CS by co-precipitation with polymeric Schiff's base resulting from the

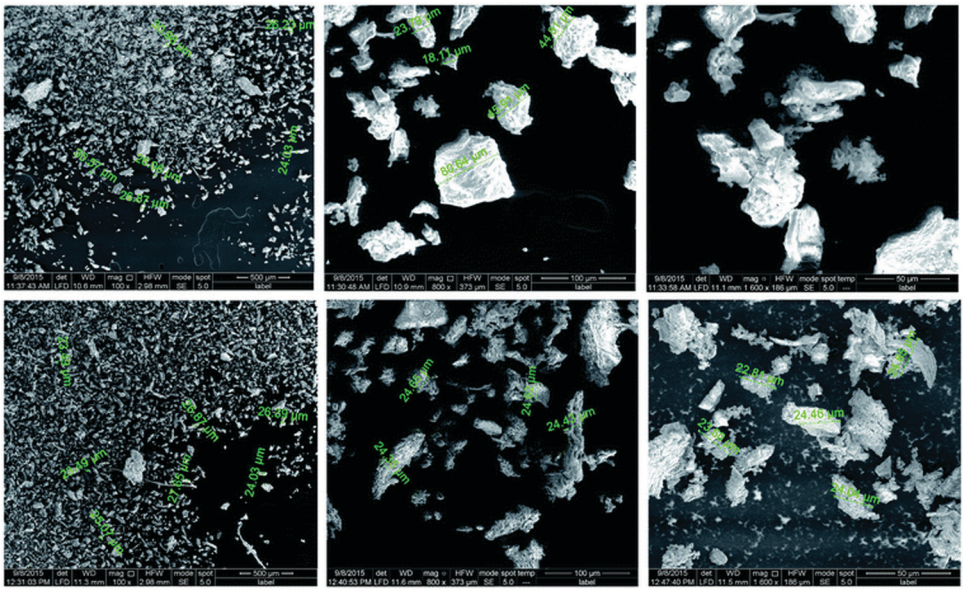

Fig. 8 SEM images of unloaded MCS–GMA-I (top), and loaded MCS–GMA (bottom).[67]

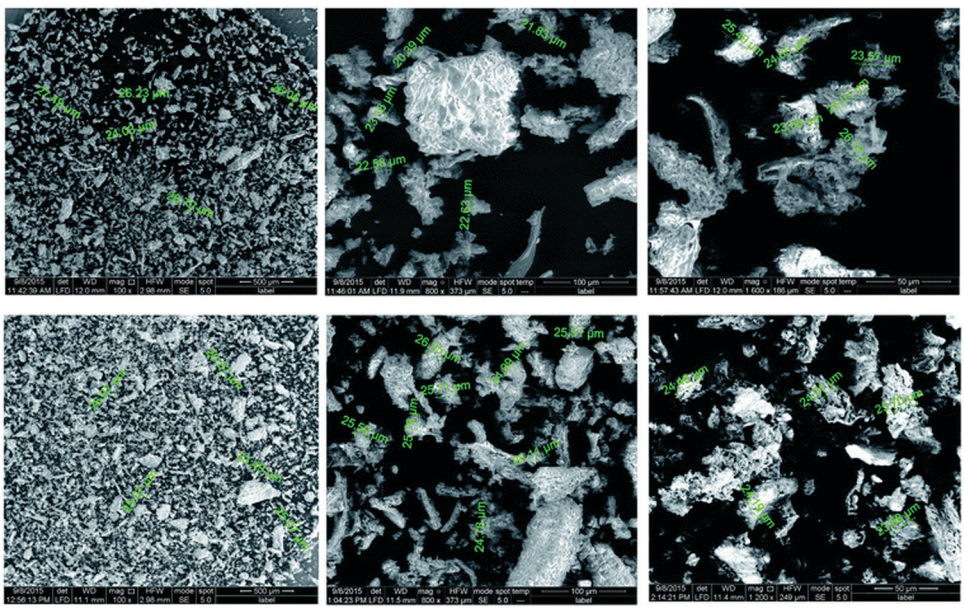

Fig. 9 SEM images of unloaded MCS–GMA-II (top), and loaded MCS–GMA-II (bottom).[67]

reaction of thiourea with glutaraldehyde. This material has great potential as a high-effective sorbent for Remazol Brilliant Blue R (RBBR). The maximum sorption capacity reached 0.441 mmol g^{-1} (0.626 mg g^{-1}) at pH 1.6 and 25 °C. Kinetic plots, pH dependence, isotherm data, and influences of ionic strength were reported. The data from equilibrium sorption experiments are well fitted to the Langmuir isotherm and the PSO sorption kinetics indicate that chemisorption controls the process. The distribution coefficient was calculated at different temperatures and the thermodynamic parameters have been calculated. The sorption reaction is endothermic, spontaneous, and increases the entropy of the system. Alkaline solution (0.5 M NaOH) was used for desorbing RBBR from loaded sorbent.[68] The sorbent exhibited good renderability over several repeated adsorption–desorption cycles.

In another study, Elwakeel's team synthesized a resin from CS and glutaraldehyde (CS–GA).[69] The resin was also chemically modified using ammonium hydroxide to produce a resin (R), which was additionally semi-cross-linked with epichlorohydrin through the hydroxyl groups of CS. The obtained resin was modified with 3-amino-1,2,4 triazole-5-thiol to produce resin R′, or melamine to produce resin R″. The uptake of the

modified CS resins toward brilliant blue R-250 (BBR-250) from aqueous media was studied using the batch method. Various parameters such as the pH, agitation time, and the temperature were studied. The resins showed a high affinity for the adsorption of BBR-250 from aqueous media, and uptake values of 0.97, 0.79, and 2.505 mmol g^{-1} were reported for resins R, R′, and R″ at 25 °C, respectively. Both the kinetic and thermodynamic parameters of the process were estimated. These data indicated an endothermic spontaneous adsorption process that kinetically followed the PSO model, Fickian diffusion low, and the Elovich model. Desorption of BBR-250 from the prepared resins was efficiently done using sodium hydroxide.[69]

Magnetite–CS composite particles were prepared *via* the *in situ* partial oxidation of ferrous ions uniformly dispersed in the polymer solution, followed by matrix precipitation under alkaline conditions and cross-linking through the addition of glutaraldehyde (GA).[70] The obtained material was characterized regarding the average particle size, saturation magnetization, crystallinity, morphology, and composition. Its potential as a non-expensive, environmentally friendly adsorbent for removal of the synthetic textile dye Remazol brilliant blue (RBB) from WW was evaluated. Batch adsorption studies were conducted to optimize the pH, initial dye concentration, and contact time. The data were analyzed using adsorption isotherms and kinetic models. Desorption tests were also performed. The results proved that the composite is an efficient adsorbent that acts in a short time and reaches a high capacity. The magnetic component ensures fast separation from the liquid phase, thus holding promise for saving energy and time in an industrial setting by avoiding filtration and/or sedimentation processes.[70]

Using a water-in-oil emulsification method, a magnetic CS composite MCS–SnO_2–Fe_3O_4 was prepared by Yu *et al.*[71] for adsorbing the anionic dye reactive brilliant red (RBR) from a aqueous solutions. The physicochemical properties of the obtained material were characterized using XRD, VSM, TGA, SEM, and N_2 adsorption–desorption. The effects of contact time, solution pH, ionic strength, initial dye concentration, and temperature on the adsorption of RBR were investigated *via* batch adsorption experiments. Compared with other adsorbents, MCS–SnO_2–Fe_3O_4 showed better a adsorption performance for RBR, represented by the adsorption capacity reaching a maximum of 981.23 mg g^{-1}. The kinetic data and equilibrium adsorption behavior were well depicted by the PSO kinetic model and the Langmuir isotherm model, respectively. According to the thermodynamic characteristics, the adsorption process was spontaneous and endothermic. The probable adsorption mechanism was validated using XPS analysis, which showed that the N atoms on the composite chelated with RBR ions in solution. In addition, the MCS–SnO_2–Fe_3O_4 particles easily underwent magnetic separation and showed outstanding reusability after recycling five times. All in all, MCS–SnO_2–Fe_3O_4 was proved to be an efficient and promising adsorbent for dye removal due to its higher adsorption capacity compared with other adsorbents.[71]

Yu *et al.*[72] provided a simple one-step chemical process for the preparation of aminated magnetic CS microspheres (TETA–MCS), which were applied for adsorbing reactive brilliant red (RBR). Meanwhile, magnetic grafted microspheres (MCS–PMAA) were prepared based on magnetic CS microspheres *via* a surface-initiating single-bond system NH_2–$S_2O_8^{2-}$ for adsorbing methylene blue (MB). The physical properties and structure of the obtained microspheres were characterized using FT-IR spectroscopy, SEM, XRD, TGA, and a vibrating sample magnetometer (VSM), and their adsorption performance for the removal of organic dyes MB and RBR was also investigated. The composite MCS–PMAA showed an excellent performance for MB, represented by the adsorption capacities reaching a maximum of 211.22 mg g^{-1} at pH 12. On the other hand, TETA–CS demonstrated remarkable adsorption properties for RBR, represented by the adsorption capacities reaching a maximum of 637.41 mg g^{-1} at pH 2. Kinetic analyses and the equilibrium adsorption behavior of dye WW onto the CS microspheres were investigated using various models. The adsorption mechanism was further analyzed *via* X-ray photoelectron spectroscopy (XPS), and it was found that the adsorption was mainly driven by hydrogen bonding and electrostatic interactions.[72]

Hu *et al.*[73] prepared and used ethylenediamine (EDA)-modified magnetic CS microspheres (EDA–MCS) for the adsorption of reactive brilliant red X-3B (RBR), reactive light yellow K-6G (RLY), and reactive brilliant blue X-BR (RBB). The EDA–MCS material showed a good adsorption performance for RBR and RLY. When the pH was 5.3–5.8 at 25 °C and the initial concentration was 200 mg L^{-1}, the adsorption capacity for RBR and RLY reached 98% and the maximum adsorption quantity achieves was 198.99 and 122.2 mg g^{-1}, respectively. The adsorption capacity of RBB on EDA–MCS was non-ideal (<10%). The adsorption isotherm of RBR was fitted by both Langmuir and Freundlich equations, and the adsorption isotherm of RLY turned out to be more in agreement with the Langmuir equation. The adsorption process follows a PSO kinetic model for both RBR and RLY.[73]

5.3. Chitosan composites

Zhang *et al.*[74] reported the statistical physics modeling of the adsorption of three dyes, brilliant blue (BB), sunset yellow (SY), and tartrazine (TT), onto CS from an aqueous solution. A multilayer statistical physics model was applied to understand the dye adsorption at different temperatures (*i.e.*, 25–55 °C) and pH 3. Modeling results showed that the adsorption was occurred with a horizontal position of the BB, SY, and TT molecules on the CS surface. The dye-adsorption capacities ranged from 406.19 to 814.27 mg g^{-1} for BB, from 924.88 to 1432.98 mg g^{-1} for SY, and from 611.27 to 1065.55 mg g^{-1} for TT. Overall, CS showed the highest adsorption capacity in the order for SY, TT, and BB. Analysis of the adsorption energies indicated that the removal of these dyes was an exothermic process, which could be governed by steric parameters according to the results obtained with the multilayer statistical physics model.[74]

The coexistence of organic dyes in WW has highlighted the great necessity to develop amphoteric adsorbents for their simultaneous removal. An amphoteric composite sponge was successfully fabricated by combining CS with electro-spun

sodium alginate nanofibers using lyophilization in acetic acid–water–dioxane mixed solvents,[75] which possessed abundant functional groups and a superior microstructure of interconnected pores and nanoscale fibers, beneficial for improvement of the adsorption capacity. The optimum adsorption capacities for acid blue 113 (AB113) and rhodamine B (RH) were 926.2 ± 25.7 mg g^{-1} and 695.4 ± 17.0 mg g^{-1}, respectively, much higher than those of the control samples prepared with CS and non-electro-spun sodium alginate in traditional acetic acid–water solvents. Meanwhile, the sponge provided a superior adsorption performance under various pH environments and for several adsorption cycles. Importantly, it showed a considerable simultaneous adsorption capacity for a binary system that contained organic dyes. Overall, the CS electro-spun sodium alginate nanofiber composite sponge showed potential for complex-WW treatment.[75]

Baburaj *et al.*[76] developed composite membranes from polyamide microfiltration membranes using a combination of the ethyleneimine (EI), CS, and acrylic acid (AA) polyelectrolyte through layer-by-layer assembly. The removal efficiency of these membranes was investigated using two model textile effluents, methylene blue (MB) and Coomassie brilliant blue (CBB). The uptake of dye was found to be very much dependent on the type of bilayer. The amount of MB uptake by the multilayer was high with the AA–CS bilayer and was influenced by the conformation of the dye within the multilayer. The initial concentration of CBB decreased from 14.75 to 1.5 mg L^{-1} and MB from 14.4 to 2.6 mg L^{-1} with a 20-bilayer membrane. An alkaline effluent pH resulted in 79.9% MB and 87.1% CBB removal. Desorption studies of MB and CBB using 19.5–20 bilayer AA–EI and AA–CS multilayers showed a pH-dependent release. Complete desorption of MB was observed at low a pH (*i.e.*, 3). In the case of CBB, enhanced desorption took place at pH 7. The chemical oxygen demand (COD) values showed a significant reduction after treatment with AA–CS multilayers.[76]

Masilompane *et al.*[77] synthesized a nanoadsorbent from Kraft lignin derived from paper and pulp black liquor, CS, and TiO_2 (T) used to remove brilliant black dye (BK) from aqueous solutions. TEM measurements confirmed that the material was nanoscale, and BET studies showed a pore width of 11.36 nm with a BET surface area of 10.75 m^2 g^{-1}. The presence of –NH, –O– and Ti–O functional groups was confirmed *via* ATR-FT-IR, and TGA indicated that the nanoadsorbent was thermally stable up to 300 °C. SEM showed that lignin had larger particles with well-defined edges, while the surface morphology of CS showed non-uniform, short fibrous microstructures. The diffraction patterns of the nanocomposite showed a polycrystalline anatase phase, and selected area electron diffraction analysis showed that the nanocomposite had small spots making up a ring, indicating that the nanoparticles have a crystalline structure. The effects of the contact time, solution pH, adsorbent dosage, and initial dye concentration on the adsorption of BK were investigated. The batch adsorption data obeyed the Freundlich isotherm, and the monolayer adsorption capacities were calculated using the linear Langmuir isotherm. The adsorption kinetics data were described by the PSO kinetic model.[77]

Metin *et al.*[78] prepared and characterized CS–zeolite (CS–Z) bio-composite beads and utilized them as adsorbents for removal of the anionic dye acid black 194 (AB194). Characterization studies on the composite beads were carried out using FT-IR, TGA, and SEM-EDX. The ability of the CS–Z composite beads to act as an adsorbent for the removal of AB194 from an aqueous solution was investigated under various experimental conditions. The maximum adsorption capacity of the composite beads was calculated as 2140 mg g^{-1}. The increase in temperature resulted in a higher AB194 loading per unit weight of CS–Z beads. As an additional factor affecting the adsorption behavior of AB194, the effect of ionic strength was investigated, and the adsorption capacity was significantly decreased. Four isotherm models were employed to elucidate the adsorption process. The most appropriate model for the equilibrium process was the Freundlich isotherm. Kinetics studies indicated that the adsorption of AB194 followed PSO kinetics. Thermodynamic calculations showed that the adsorption of the reactive dye was a spontaneous and endothermic process. The obtained results indicate that CS–Z beads as an adsorbent are promising for the removal dye from WW.[78]

It is important to devise new strategies for deriving value from low-cost materials, for example, lignin, which is a potential waste by-product from the paper industry and present-day biorefineries. Nair *et al.*[79] reported the facile preparation and characterization of a range of CS–alkali lignin (CS–AL) composites for the removal of organic dyes present in WW. The composites were characterized by the presence of weak bonding between the beta-1,4-glycosidic linkage, and amide and (–OH) groups of CS, and the ether and hydroxyl groups of alkali lignin. Various reaction parameters, like the CS content in the composite, the initial pH, and the adsorbent dosage, were optimized. Batch adsorption studies showed that the CS–AL (50 : 50) composite exhibited a maximum percentage removal of anthraquinone dye (AQ), and Remazol brilliant blue R (RBBR), compared with other CS–AL composites. The adsorption of RBBR on the composite followed the Langmuir isotherm and PSO kinetics. A mechanism of adsorption that involves: (I) the electrostatic interaction of protonated amino and hydroxyl groups of the composite with anionic SO^{3-} and $HCrO^{4-}$ groups of the dye, and (II) chemical interaction between amino and hydroxyl groups of the composite, and the carbonyl moiety of the dye, was proposed. The surface morphologies of the CS, alkali lignin, 25-CS–AL, and 50-CS–AL composites studied using SEM are shown in Fig. 10. It is observed that the surface of CS is non-uniform and rough with short fibrous structures, while the alkali lignin particles are larger with sharp edges and a lower surface roughness. From the SEM images of the 25-CS–AL and 50-CS–AL composites in Fig. 10(c and d), the interfacial adhesion that binds the CS flakes on the lignin surface is very clear.[79]

In another research article, Nitayaphat[80] investigated the adsorption performance of CS beads after coffee residue (CR) blending for the removal of reactive red 152 (RR152) as an anionic dye. The study of dye removal using the CS–CR composite beads as a function of the CR concentration indicated

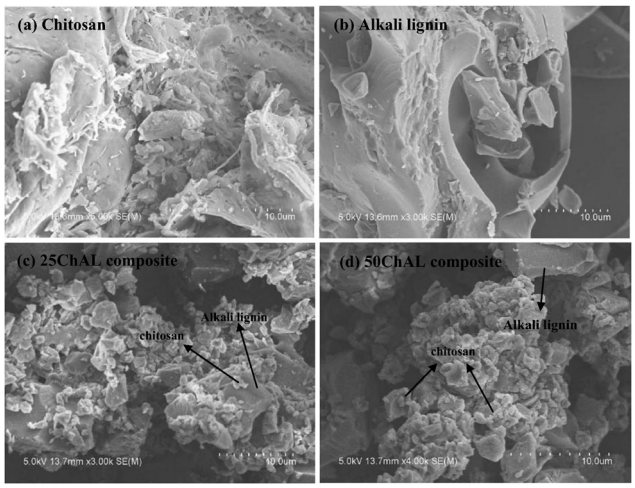

Fig. 10 SEM images of (a) CS, (b) AL, (c) 25-CS–AL composite, and (d) 50-CS–AL composite.[79] Reproduced from ref. 79, with permission from Elsevier, 2014.

that the CS-to-CR mass ratio of 60/40 was the most useful for enhancing the dye removal. The effects of contact time, initial pH, and adsorbent dosage on the adsorption efficiency were investigated systematically. The equilibrium adsorption isotherm of the CS–CR composite beads exhibited a better fit to the Langmuir isotherm model than to the Freundlich isotherm model. The maximum adsorption capacity of the composite beads was 4.27 mg g^{-1}. The dye desorption of the composite beads was 24.83%. SEM images confirmed that after adsorption the dye was dispersed onto the composite-bead surface. This study demonstrated that the CS–CR composite can effectively remove reactive dye from an aqueous solution simply and with a low cost.[80]

Şenol *et al.*[81] used a CS–vermiculite (V) composite-bead material, which is a low-cost and naturally effective adsorbent, for the efficient removal of sunset yellow (SY) and brilliant blue (BB) food dyes from aqueous solution. The CS–V composite beads were characterized using FT-IR, SEM, XRD, and point-of-zero-charge (PZC) analysis. The adsorbent properties of the CS–V composite beads for SY and BB dyes were evaluated in terms of the pH, concentration, kinetics (time), and thermodynamics (temperature) of adsorption. The experimental data presented were obtained from Langmuir, Freundlich, and Dubinin–Radushkevich isotherm models. The maximum adsorption capacity for the Langmuir equation was found to be 0.387 mol kg^{-1} for SY and 0.229 mol kg^{-1} for BB. The results showed that the experimental data were best fitted by the Langmuir model for SY and the Freundlich model for BB. Adsorption energies obtained from the DR model for SY and BB showed that the adsorption processes were chemical. As a result of the thermodynamic evaluation of SY and BB adsorption, it was found that the adsorption processes were endothermic, entropy increased, and the reaction was spontaneous.[81]

The eco-friendly polymer–bio-polymer composite polyaniline–CS (PAN–CS) as an adsorbent was tested for the removal of Congo red (CR), Coomassie brilliant blue (CBB), Remazol brilliant blue R (RBBR), and methylene blue (MB) from aqueous solutions.[82] SEM showed that the surface of the composite was rough with pleats, providing good conditions for dye adsorption. XRD of the composite showed the main reflections of both CS and PAN. Experiments were carried out as a function of the contact time, for an initial dye concentration of 100 mg L^{-1}, at pH 3, and an adsorbent dose of 100 mg L^{-1}. The maximum percentage removal was found to be 95.4% for CR, 98.2% for CBB, and 99.8% for RBBR. The Langmuir model showed a satisfactory fit to the equilibrium adsorption data of the PAN–CS composite. The kinetics of the adsorption followed a PSO rate expression, which demonstrates that intraparticle diffusion plays a significant role in the adsorption mechanism. FT-IR and desorption studies confirmed the involvement of amino and hydroxyl groups in the dye adsorption.[82] These results indicate that the polymer matrix can be used as an adsorbent for the removal of sulfonated dyes from aqueous solutions.

According to Karaer and Uzun,[83] the capability of CS to adsorb basic dyestuffs is very low. For this purpose, CS was modified to increase its adsorption capability with some cyclic acid anhydrides (AA) in dimethyl sulfoxide (DMSO). Then, CS modified with maleic anhydride (CS–MA), CS modified with phthalic anhydride (CS–PA), and CS modified with trimellitic anhydride (CS–TA), were compared according to their capabilities for removing brilliant green (BG) and methylene blue (MB) from aqueous solutions. It was determined that CS–TA adsorbed much more BG and MB. 70.57% of BG and 71.86% of MB in samples of 50 mL using 100 mg CS–TA were adsorbed at room temperature and a shaking rate of 140 rpm within 24 h. As a result of this, the adsorption of BG and MB by CS–TA was kinetically investigated as being dependent on the temperature and pH.[83]

Le and Shimoyama[84] focused on the adsorption kinetics and isotherm modeling in CO_2-activated CS (CO_2-CS). The removal efficiency and adsorption capacity were measured for brilliant blue FCF (BBF), Congo red (CR), and orange II (O-II), and the highest removal efficiencies of BBF, O-II, and CR were 97%, 91%, and 48%, respectively. The adsorption in the CO_2-CS was found to follow the PSO model. The activation of adsorption by CO_2 was found to lead to a higher adsorption rate constant and a higher adsorption capacity due to protonation of the CS amino groups. Interestingly, as the temperature of the CO_2-CS was increased, the PFO model predicted a decrease in the adsorption rate constant, k_1. This is thought to be a result of lower CO_2 dissolution into the aqueous solution, which leads to a slower protonation process of the CS adsorption sites. The chemical structure of the dye species affects the adsorption kinetics in CO_2-CS. There are four charged functional groups on the CR molecule and three on the BBF molecule, which enables faster alignment onto the adsorption sites compared with O-II molecules that have only one charged group. In terms of the adsorption isotherm, BBF adsorption was found to follow the Langmuir model in CO_2-CS.[84]

Mixed azo dyes present in various effluents may often impair the adsorption efficiency, thereby calling into question the

applicability of the adsorbent in a real-time scenario. The simultaneous adsorption of acid yellow 36 (AY36) and acid blue 74 (AB74) from their aqueous solutions onto graphene oxide (GO) nanoplatelets embedded in a CS matrix (GO–CS) under ultrasound exposure was investigated.[85] The results obtained were subjected to analysis for the process isotherms, kinetics, and thermodynamics. This process was also optimized for the best results using response surface methodology (RSM) and modeled using an artificial neural network (ANN). The nanocomposite was characterized both before and after adsorption using FT-IR, SEM, TEM, and AFM. Under the experimental conditions prescribed by RSM, 500 mg L^{-1} of adsorbent was responsible for 98.18% and 98.80% of the removal of AY36 and AB74, respectively, when exposed to 6.48 min of ultrasonic irradiation. Hence, ultrasound-assisted GO–CS proved to be a cost-effective and sustainable adsorbent that is effective in low dosages and significantly reduced times with possible applications for the treatment of real industrial effluents that are rich in mixed dyes.[85]

A double-cross-linked biohybrid aerogel bead biosorbent made from waste bamboo paper and CS (BHA–CS) was prepared by sequential physical and chemical cross-linking.[86] The resulting BHA–CS beads were applied to remove methylene blue (MB) and Congo red (CR) dyes in both single and binary systems. The MB and CR adsorption capacities of the BHA–CS beads increased with increasing adsorbent dosage, contact time, temperature, and initial dye concentration. With increasing solution pH, the MB adsorption capacity increased, while that for CR increased initially and then decreased. The maximal adsorption capacities for MB and CR were 653.3 and 559.6 mg g^{-1}, respectively, in the single system. The thermodynamic analysis results showed a spontaneous and endothermic adsorption process. The BHA–CS beads showed good stability and re-usability with removal efficiencies of 49.4% and 60.6% for MB and CR, respectively, after five cycles of adsorption–desorption. For the binary system, the adsorption of MB was inhibited by CR, while the removal of CR was enhanced by MB.

In another study,[87] CS beads bi-functionalized with the ionic liquid Aliquat 336 (ALI336) and anionic surfactant cetyltrimethylammonium bromide (CTMAB) were prepared and characterized using different techniques, including FT-IR, XRD, SEM, EDS, and BET surface-area analysis. Characteristic analysis confirmed the successful conjugation of CS–ALI336–CTMAB. The novel fabricated CS–ALI336–CTMAB beads were efficiently used as a high-performance adsorbent for the removal of tartrazine (TT), an anionic food dye, from polluted water. The optimum adsorption of TT onto the CS–ALI336–CTMAB beads was found to be 2000 mg L^{-1} of adsorbent in the wide pH range of 4–11, whereas just 45 min was required to reach more than 90% adsorption efficiency under the studied conditions. In addition, adsorption and kinetics studies showed that the experimental data fitted well the PSO kinetic model and the Langmuir isotherm model, respectively. The maximum adsorption capacity of the prepared beads was found to be 45.95 mg g^{-1} at 45 °C.[87]

There has been an increasing trend for developing various low-cost grafted natural amino polysaccharides for the absorption and removal of malachite green (MG) and reactive red–195 (RR195) dyes from aqueous solution. A promising non-toxic biosorbent that possesses a high charge density and thermal stability was prepared using hexametaphosphate (HMP) as an ionic cross-linker.[88] Batch adsorption experiments were carried out at different temperatures (25, 35, and 45 °C), pH conditions (2–10), adsorbent dosages (0.01–0.1 g), and contact times of up to 180 min to understand the optimum experimental conditions and simultaneously evaluate the adsorption isotherms and kinetics of CS–HMP. The biosorption equilibrium was established in 120 and 60 min for the removal process of MG and RR195, respectively. The pseudo-equilibrium process was best described by the PSO kinetic, Freundlich and Temkin isotherm model. The removal rate of MG and RR195 gradually increased to 69.40 and 148 mg g^{-1}, respectively, at the contact period of 50 min in a single-contaminant system, although the removal efficiency of the acid dye was ~2 times higher compared with the basic dye under the optimum conditions. The thermodynamic parameters indicated the exothermic MG and endothermic RR195 nature of spontaneous dye removal. Therefore, the obtained results validate the sustainable utilization of CS–HMP as promising functionalized CS microparticles for removing dye effluents from contaminated aqueous phases.[88]

The preparation of a polyaniline/silica nanostructure (PSn) in chitosan/polyvinyl alcohol nanofibers (CP) was evaluated to enhance the CP dye-removal capacity.[89] FT-IR, field-emission scanning electron microscopy (FE-SEM), and energy-dispersive X-ray spectroscopy (EDS) results confirmed the chemical grafting of silica on the polyaniline nanoparticles. BET results showed a specific surface area of 61 m^2 g^{-1} for the studied sorbent. The adsorption capacity of the nanofibers increased from 48 to 110 mg g^{-1}, from 40 to 90 mg g^{-1}, and from 31 to 45.2 mg g^{-1} for Congo red (CR), methyl orange (MO), and methylene blue (MB) dyes, respectively. The CR and MO uptake was observed at pH 5, while for MB the optimum uptake was detected at pH 9. Isotherm experimental results showed that the Sips isotherm model could well describe the adsorption process. Thermodynamics studies at 25 and 55 °C verified that the adsorption process is spontaneous. The highest recovery after 5 cycles was observed for NaOH solution (0.1 M), which was 74, 68, and 55% of the adsorption capacity of the first cycle for the CR, MO, and MB dyes, respectively.[89]

5.4. Comparison of different chitosan derivatives in dye removal

Table 4 compares the different CS modifications in dye removal and shows the differences in pH, temperature, adsorption capacity, nature of the adsorption, dyes, and kinetic models and isotherms.

6. Bibliometric analysis of anionic dye removal by CS

The subject ''Anionic dye removal by chitosan'' was used to search the Web of Science (WOS) database for publications on CS (retrieved on 28/02/2022). The study was conducted from

Table 4 Comparison of different CS modifications in dye removal

Adsorbent	Dye	pH	Temp. (C)	Nature of adsorption	Adsorption capacity (mg g^{-1})	Kinetic model	Isotherm	Ref.
CS-modified magnetic graphitized multi-walled carbon nanotubes	Congo red	6	25	Exothermic	263.3	PSO	Langmuir	90
Maghemite nanoparticles are encapsulated in the cross-linked CS beads	Methyl orange	4	20	—	779	PSO	Langmuir	91
Modified CS resin R	Reactive black 5	3	25	Endothermic	0.63	PSO	Langmuir	92
Modified CS resin R′	Reactive black 5	3	25	Endothermic	0.78	PSO	Langmuir	92
Glutamic acid-modified CS magnetic composite microspheres	Methylene blue, crystal violet, light yellow 7GL	7	20	—	182.5, 403.2, 236.4	PSO	Langmuir	93
Chitosan magnetic composite microspheres	Methylene blue, crystal violet, light yellow 7GL	7	20	—	33.6, 86.6, 26.3	PSO	Langmuir	93
Magnetic CS and graphene oxide	Methylene Blue	5.3	30	Exothermic	95.31	PSO	Langmuir	94
Fe_3O_4–zinc oxide–CS	Amaranth, tartrazine	2	—	—	99.6, 47.3	PSO	Freundlich	95
N-Benzyl-*O*-carboxymethyl CS magnetic nanoparticles	Methylene blue, crystal violet, malachite green	7	60.15	Endothermic	223.58, 248.42, 144.79	PSO	Langmuir, Freundlich	96
Glutaraldehyde cross-linked magnetic CS beads	Direct red 23	4	25	—	1250	—	Langmuir	97
Magnetic γ-Fe_2O_3/cross-linked CS composites	Methyl orange	6.6	27	—	—	PSO	—	98
Graphite oxide with magnetic CS	Reactive black 5	3	65	Endothermic	425	PSO	—	99
Magnetic β-cyclodextrin–CS–graphene oxide	Methylene blue	—	—	Endothermic	84.32	PSO	Langmuir	100
Magnetic CS–poly(vinyl alcohol) hydrogel beads	Congo red	5	25	Endothermic	470.1	PSO	Langmuir	101
Magnetic composite CS-coated magnetic Fe_3O_4 particles	Congo red	2	42	Endothermic	56.66	—	Langmuir	102
Chitosan-wrapped magnetic nanosized γ-Fe_2O_3/multi-walled carbon nanotubes	Methyl orange	3–6	24	Exothermic	66.09	PSO	Langmuir	103
Magnetic maghemite–CS nanocomposite films	Methyl orange	2	57	Exothermic	29.41	PSO	Langmuir	104
Magnetic N-lauryl CS	Remazol red 198	—	25	Endothermic	267	PSO	Langmuir, Freundlich	105
γ-Fe_2O_3–SiO_2–CS composite	Methyl orange	5	37	Exothermic	34.29	PSO	Langmuir	106
Magnetic β-cyclodextrin–CS nanoparticles	Methylene blue	5	30	Exothermic	2.78	PSO	Langmuir	107
Carboxymethylated CS-conjugated magnetic nano-adsorbent	Acid orange 12, acid green 25	3	25	Endothermic	1883, 1471	PSO	Langmuir	108
CS-coated magnetite nanoparticles	Reactive yellow 145	3	45	Endothermic	70.10	PSO	Langmuir	109
CS coating on the surface of magnetite	Alizarin red	3	30	Exothermic	43.08	PSO	Langmuir	110
Xanthated CS–cellulose sponges	Congo red, methylene blue	3–9	30	Exothermic	120	PSO	Langmuir	111
Cross-linked CS	Malachite green, indigo carmine	6–9	40	—	714.29	PSO	Langmuir	112
CS nanofibers modified by mesoporous silica sieve	Brilliant red	7	—	—	—	PSO	Langmuir	113
CS	Brilliant blue, sunset yellow, tartrazine	3	25	Exothermic	814.27, 1432.98, 1065.55	—	Langmuir	74
Polyaniline–CS	Congo red, Coomassie brilliant blue, Remazol brilliant blue R, methylene blue	3	—	—	322.58, 357.14, 303.03	PSO	Langmuir	82
CS–sodium alginate	Acid black–172, methylene blue	3–11	25	Endothermic	817, 1488.1	PSO	Langmuir	114
Polypyrrole-decorated CS-based magsorbent	Crystal violet, methyl orange	3–12	30	Exothermic	62.89, 98.29	PFO	Langmuir	115
Diatomite-CS–Fe(III) composite	Direct yellow R, Congo red, methyl orange, direct red 23	6–12	25	Exothermic	833.3, 1250, 1000, 1000	PSO	Langmuir	116
Polystyrene–CS	Reactive red 24, Congo red	2–12	25	—	—	PSO	Langmuir	117
Schiff base–CS-grafted L–monoguluronic acid	Congo red	6	30	—	459.75	PSO	Langmuir	118
CS-multiwalled carbon nanotube beads	Congo red, methylene blue	5	30	—	450.4	PFO	Langmuir	119
Cellulose acetate–CS–single-walled carbon nanotubes–ferrite–titanium dioxide	Congo red, methylene blue	2–3	—	—	74.2	PSO	Langmuir	120
CS–zeolite composite	Reactive red 120, reactive red 196	5	—	—	19.6, 39.021	PSO	Hill, Sips and Jovanovic	121
Cross-linked CS–tripolyphosphate–fly ash composite	Reactive red 120	4	45	Exothermic	165.8	PSO	Freundlich	122

Table 5 Number of publications according to Web of Science categories (subjects)

Web of Science category	Record count	Percentage of 624 publications
Polymer science	170	28.96
Engineering chemical	140	23.85
Chemistry applied	112	19.08
Engineering environmental	104	17.71
Environmental sciences	101	17.20
Chemistry multidisciplinary	78	13.28
Chemistry physical	75	12.77
Biochemistry molecular biology	67	11.41
Water resources	60	10.22
Chemistry organic	83	6.47

1900 to 2022. During the timeframe 1900–2022, a total of 624 publications was collected from WOS. The categories of polymer science, engineering chemical, chemistry applied, engineering environmental, and environmental sciences accounted for 28.96%, 23.85%, 19.08%, 17.71%, and 17.20%, respectively, of all 624 CS publications (Table 5). From 1989 until 2006, CS publications were rare. Since 2007, there has been an increase in the number of papers. With 93 papers, the year 2020 was the most productive, followed by 2021 and 2019 with 88 and 79 papers, respectively (Fig. 11). In terms of countries with CS publications, The People's Republic of China had the most, at 226 out of 624 (36.21%), followed by India, at 65 (10.41%). Iran published 58 papers (9.29%), followed by Egypt with 35 papers (5.60%) (Fig. 12).

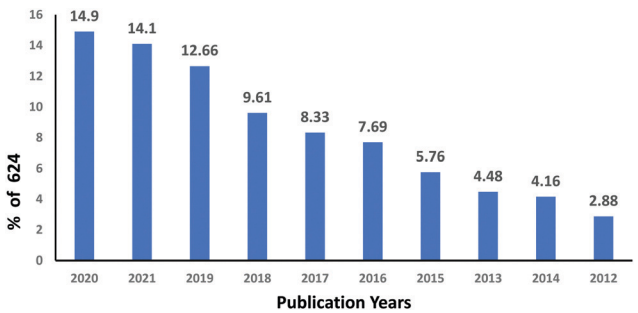

Fig. 11 Number of publications on anionic dye removal by CS through the years.

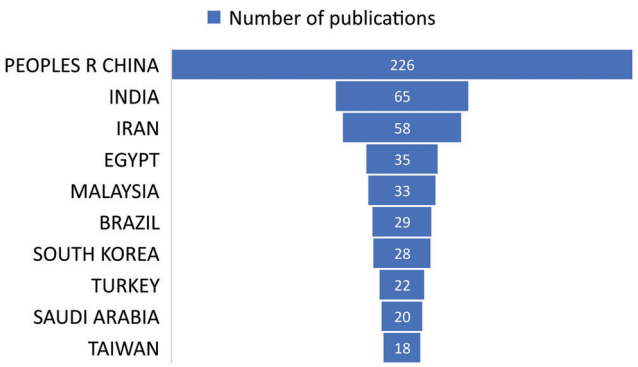

Fig. 12 Most countries published work on the topic of anionic dye removal by CS.

7. Glycidyl methacrylate

Glycidyl methacrylate (GMA) is the most used monomer because of its epoxy groups. The chemical structure of the GMA monomer is shown in Fig. 13. Other chemical groups such as carboxyl, amide, amine, and hydroxyl react easily with the epoxy ring. Glycidyl methacrylate copolymers treated with amine groups such as ethylenediamine and diethylenetriamine adsorb heavy-metal ions and anionic–cationic dyes well.[123]

Glycidyl methacrylate/methelenebisacrylimide resin loaded with tetraethelenepentamine ligands was prepared and investigated.[17] The adsorption characteristics of the obtained resin towards reactive black 5 (RB5) from aqueous solutions under different experimental conditions were established through batch and column methods. The mechanism of interaction between RB5 and resin's active sites was discussed. The resin showed a high affinity for the adsorption of RB5 where an uptake value of 0.63 mmol g^{-1} was reported for the obtained resin at 25 °C. The kinetics and thermodynamic behavior of the adsorption reaction was also defined. These data indicated an endothermic spontaneous adsorption process that kinetically followed the PSO model. Breakthrough curves for the removal of RB5 were studied at different flow rates and bed heights. The critical bed height for the studied resin column was found to be 0.764 cm at a flow rate of 8 mL min^{-1}. The adsorbed dye was eluted from the investigated resin effectively. The regeneration and durability of the loaded resin towards the successive resin were also clarified.[17]

In a similar study, the macroporous GMA and ethylene glycol dimethacrylate copolymer (EGDMA) functionalized with diethylene triamine (GMA/EGDMA–DETA) was evaluated as a sorbent for reactive black 5 (RB5).[124] Batch RB5 removal from aqueous solution by GMA/EGDMA–DETA was investigated by varying the pH, contact time, sorbent dosage, initial dye concentration, and temperature. The sorption is pH sensitive and has a maximum at pH 2 (dye removal of 85%), decreasing with the increase in pH (dye removal of 24% at pH 11) after 60 min. The PSO kinetic model accurately predicted the RB5 amount sorbed under all investigated operating conditions, while intraparticle diffusion was the dominant rate-limiting mechanism. The diffusion mechanism was more enhanced with a decrease in temperature and an increase in concentration. The isotherm data were best fitted using the Langmuir model, indicating the homogeneous distribution of active sites on GMA/EGDMA–DETA and monolayer sorption, with the maximum sorption capacity of 353 mg g^{-1}. The calculated sorption rates improved with increasing temperature and an activation energy close to 40 kJ mol^{-1} was determined, suggesting that chemisorption was also rate-controlling.[124]

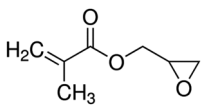

Fig. 13 Glycidyl methacrylate (GMA) structure.

Elwakeel *et al.*[125] prepared magnetic sorbent microgranules with a magnetite (Fe_3O_4) core and a GMA–*N*,*N*′-methylenebisacrylamide shell (MGMA–*N*,*N*′-MBA). Diethylenetriamine (DETA) was successfully grafted onto the magnetic microgranules to obtain a sorbent (MGMA–*N*,*N*′-MBA–DETA) with a very high content of amino groups. The obtained sorbent MGMA-*N*,*N*′-MBA–DETA was characterized *via* FT-IR spectroscopy, SEM, TEM, XRD, TGA, and vibrating sample magnetometry (VSM). This material showed a high affinity for the uptake of acid yellow 99 dye (AY99) from aqueous solutions: the maximum sorption capacity reached 0.25 mmol g^{-1} at pH 3 and ambient temperature (*i.e.*, 25 ± 1 °C). The best results were respectively obtained with the PSO rate equation and the Langmuir equation. The distribution coefficient was obtained at different temperatures and the thermodynamic parameters were calculated. The sorption is endothermic, spontaneous, and contributes to the increasing the entropy of the system. NaOH solution (1.0 M) was used for AY99 desorption from loaded sorbents, and the sorbent could be efficiently recycled for a minimum of three sorption–desorption cycles. Therefore, MGMA–*N*,*N*′-MBA–DETA could serve as a promising adsorbent for AY99 removal from industrial WW.[125]

The macroporous GMA, methyl methacrylate (MMA) and divinylbenzene (DVB) terpolymer functionalized with diethylenetriamine tetraacetic acid (DTTA), *i.e.*, GMA–MMA–DVB–DTTA, was applied for the removal of methyl orange (MO) and methylene blue (MB), respectively.[126] The impact of several variables on the adsorption process, such as the sorbent amount, contact time, temperature, and pH, was studied. The proposed sorbent worked efficiently in real water samples with acceptable accuracy and precision. The results suggested that GMA–MMA–DVB–DTTA could be used as an effective and proper adsorbent for the removal of MB and MO from water samples.[126]

Three amino-functionalized cellulose–polyGMA graft copolymers (AM-Cell-*g*-PGMA) were tested as ion-exchange resins for the adsorption of dyes from aqueous solutions using batch techniques.[127] The three adsorbents had been prepared earlier based on the aminization of the grafted copolymer with triethylamine hydrochloride (TEAC), diethylene triamine (DETA), and triethylene tetraamine (TETA), which are represented as R1, R2, and R3 respectively. The adsorption time and the solution pH were varied. The maximum adsorption capacities of R1 were 147.5 and 150 mg g^{-1}, whereas the maximum adsorption capacities of R2 were 117.7 and 133 mg g^{-1}, and the maximum adsorption capacities of R3 were 124 and 138 mg g^{-1} for acid black 194 (AB194) and reactive black 5 (RB5) dyestuffs, respectively. It was found that the maximum adsorption capacities for the three resins decreased in the order R1 > R2 > R3 for sorption of the two dyes. Concerning these results, the R1 resin was then selected for further adsorption investigations regarding isotherm and kinetic studies. The isotherm data were well described by the Langmuir equation over the concentration range studied. The sorption kinetic parameters were determined revealing that the investigated system obeyed the PSO model.[127]

When we talk about GMA modification, the work of Köse *et al.*[128] provides a good example of modification using cellulose nanocrystals (Cell), which were used to modify poly(2-hydroxy ethyl methacrylate–GMA), giving poly(HEMA–GMA) cryogels prepared *via* base-catalyzed Cell addition. The resulting cryogels were characterized *via* FT-IR, SEM, and N_2-adsorption methods. As expected, the ability of the Cell-modified cryogels to retain water was high (~600 mg g^{-1} cryogel), leading to increased diffusion of the analyte to the adsorbent flow channels. To increase the functionality of the polymeric adsorbents towards anions, Fe(II) ions were immobilized on the polymeric adsorbent and quantified using an electrochemical method. Methyl orange (MO) was chosen as the model anionic dye molecule and adsorption studies were conducted at different pH levels, target concentrations, and times of binding. The advantages of Cell addition and Fe(II) immobilization were determined against unmodified poly(HEMA–GMA) cryogels. It was found that 455 mg g^{-1} of the Fe(II)-immobilized polymer (25% removal) was optimal for adsorption, resulting in the removal of approximately 55.75 mg g^{-1} (17.25%) for MO at a concentration of 100 mg L^{-1}. The surface morphology of the polymeric cryogels was analyzed using SEM, as shown in Fig. 14. The surface roughness increases with each additional step starting from unmodified poly(HEMA–GMA) to Cell modification and finally Fe(II) binding. Compared with neat poly(HEMA–GMA), small spots appear on the micron size scale. However, nothing that looks like Cell is visible, although the scan size is probably too large to make them out individually. Islands are also formed due to Fe(II) addition, which is beneficial for overall adsorption as this increase in surface area enables more contact for the target molecule. The higher roughness provides better adsorption zones for the target molecules.[128]

Glycidyl methacrylate cross-linked CS cryogels functionalized with negatively and positively charged molecules were prepared *via* thermo-cross-linking and freeze-drying methods.[48] These CS-based cryogels present a well-defined 3D microporous network structure with an ultra-light and highly porous nature and have a high water-absorption ability. For CS–GMA–SMA cryogels, 71.20% of cationic yellow X-8GL (CY) can be removed, and the process kinetics corresponded well to the PSO model and Freundlich model. The quantity and percentage of reactive yellow B-4RFN (RY) removed by the CS–GMA–DMC cryogel reached 224.6 mg g^{-1} and 96.11%, which closely fitted the PSO model, and the Dubinin–Radushkevich isotherm. The prepared CS-based cryogels show great potential for the remediation of dye WW samples.[48]

The epoxy groups of poly(ethylene terephthalate) (PET) copolymers grafted with GMA were modified with ethylenediamine (EDA) to form an adsorbent for the removal of Congo red (CR) and acid violet7 (AV7) in the aqueous environment.[123] The graft copolymers (GMA-*g*-PET) were synthesized with different grafting yields *via* a radical polymerization process using benzoyl peroxide (Bz_2O_2) as the radical initiator. The amination of GMA-*g*-PET fibers using EDA was studied in different solvents, and the maximum yield (w/w%) was obtained in the toluene. The grafted and modified fibers were analyzed using a CHNS organic elemental analyzer, SEM, FT-IR spectroscopy, and nuclear magnetic resonance spectroscopy (^{13}C-NMR). Through SEM analysis, the morphological changes were shown after grafting. The chemical changes after grafting and the addition of EDA to

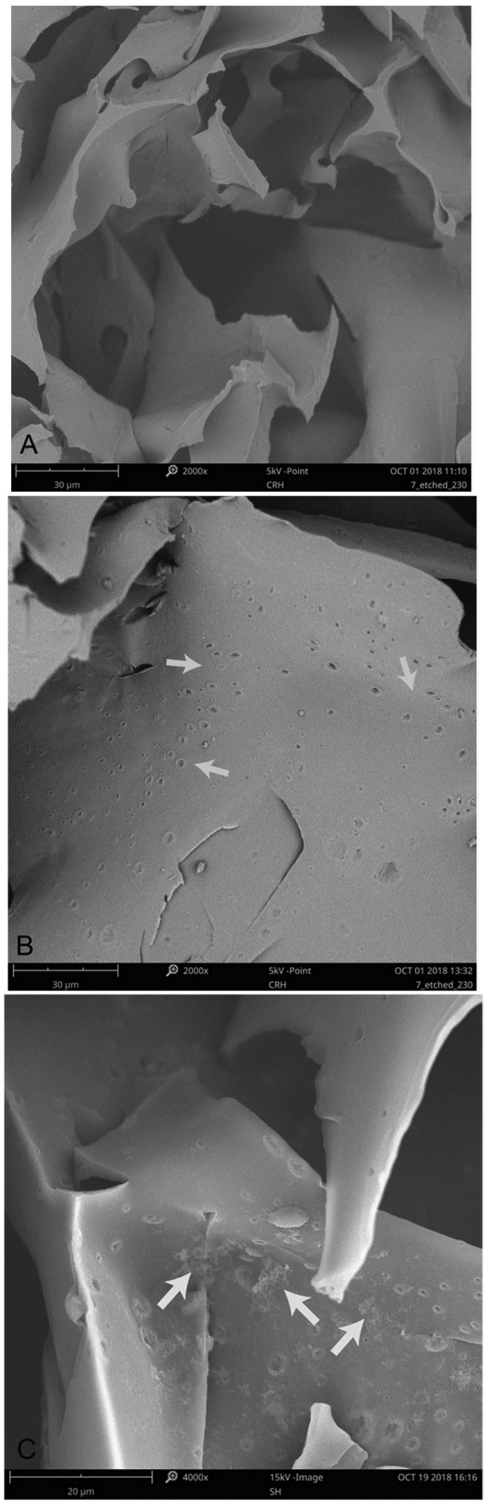

Fig. 14 SEM images of (A) unmodified poly(HEMA–GMA), (B) Cell-modified poly(HEMA–GMA), and (C) Fe(II)-immobilized poly(HEMA–GMA)–Cell cryogels.[128] Reproduced from ref. 128, with permission from Springer Nature, 2022.

the fibers were proved *via* FT-IR, NMR, and elemental analysis. The thermal properties of the grafted and aminated fibers were researched using thermogravimetric analysis and differential scanning calorimetric analysis. The removal of dyes by the EDA–GMA-*g*-PET fibers was investigated in an aqueous medium under different conditions. The optimum conditions of different parameters such as the pH of the medium, the graft yield of GMA on the fibers, the adsorption duration, the initial concentration of dye molecules, and the effect of the graft yield on the amination reaction were examined. The optimum pH for CR and AV-7 removal was found 5 and 3, respectively. The removal yield was found to be about 100% for both dyes while the initial concentration of the dyes was changed from 10 to 400 mg L^{-1}. Dyes adsorbed with the fibers were desorbed using 1 M NaOH under room-temperature conditions. The SEM photographs of the original PET fibers and the GMA-*g*-PET fibers are demonstrated in Fig. 15(a) and (b), respectively. It is obvious from the

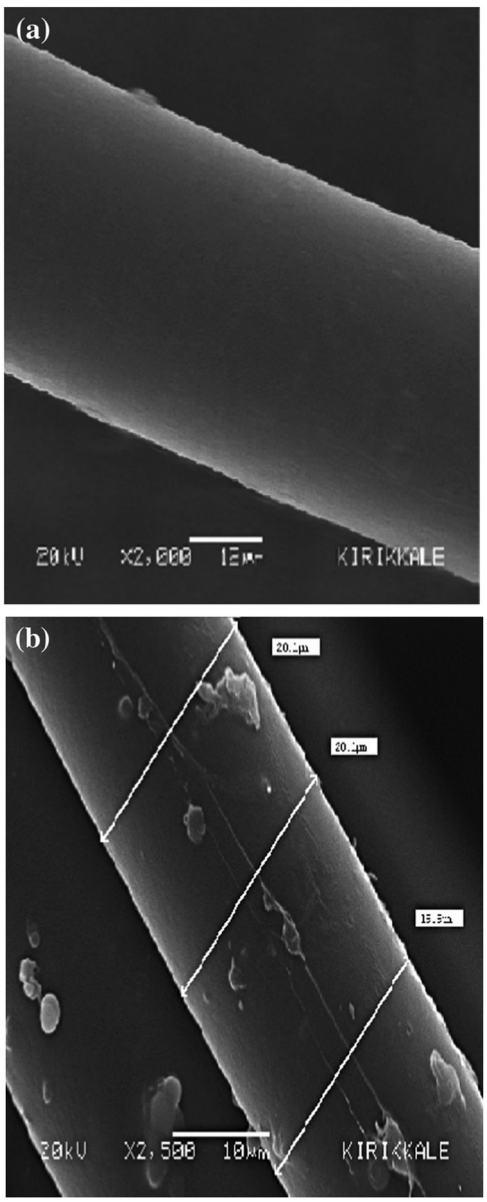

Fig. 15 SEM micrographs of (a) original PET fibers and (b) GMA-grafted PET fibers (having 150% graft yield).[123] Reproduced from ref. 123, with permission from Springer Nature, 2021.

SEM micrographs that the surface of the ungrafted PET fibers has a smooth and comparatively homogeneous morphology. Upon grafting, the GMA-*g*-PET surfaces became more heterogeneous, showing evidence of grafting.[123]

The intensive development of many industries, including those for textiles, paper, plastic, and foods, generate huge amounts of WW that contain not only toxic dyes but also harmful auxiliaries such as salts, acids, bases, surfactants, oxidants, and heavy-metal ions. The divinylbenzene (DVB) copolymer with GMA functionalized with triethylenetetramine (DVB-*co*-GMA–TETA) resin was prepared and the obtained microspheres were evaluated as a potential adsorbent for the removal of acid dye from dyeing effluents.[129] The sorption capacities were 142.4 mg g^{-1} for acid green 16 (AG16), 172 mg g^{-1} for acid violet 1 (AV1), and 216.3 mg g^{-1} for acid red 18 (AR18). Non-linear fitting of the Freundlich isotherm to the experimental data was confirmed rather than to the Langmuir, Temkin, and Dubinin–Radushkevich isotherms. The kinetic studies revealed that intraparticle diffusion is the rate-limiting step during dye adsorption. Auxiliaries such as Na_2SO_4 (5–25 g L^{-1}), CH_3COOH (0.25–1.5 g L^{-1}), and an anionic surfactant (0.1–0.5 g L^{-1}) present in the dyeing baths enhance the dye adsorption by the resin in most cases. Regeneration of DVB-*co*-GMA–TETA is possible using 1 M NaCl–50% v/v CH_3OH.[129]

Sharma and Kumar[130] functionalized cellulose (Cell) with hydroxyethyl methacrylate (HEMA) and GMA for applications in metal-ion- and dye-adsorption. The graft copolymers were used for the removal of malachite green (MG), crystal violet (CV), and Congo red (CR) dyes as a function of the adsorption time, temperature, pH of the medium, and concentration of metal ions and dyes. The sorption capacities of the polymeric adsorbents for all the adsorbates decreased in the order Cell–HEMA-*co*-GMA > Cell–HEMA > Pure cellulose. Cell–HEMA-*co*-GMA removes 49.42%, 67.74%, and 70.38% of the MG, CV, and CR dyes, respectively. The dye sorption data are best fitted using the PSO kinetic model and the Langmuir adsorption isotherm model. Before the adsorption studies the grafting reaction conditions of HEMA and GMA onto cellulose had been optimized. FT-IR, XRD, SEM, and TGA–DTA characterization techniques were used to investigate the structural aspects of the graft copolymers. The swelling properties of the graft copolymers were studied under different pH conditions.[131]

The nano-cation exchanger sulphonated polyGMA (SPGMA) was used as a sorbent material for removing one of the common organic dyes.[132] SPGMA was prepared and characterized to ensure its surface ability to sorb the dye. The percentage removal of methylene blue (MB) using SPGMA was studied by changing different parameters such as the sorbent amount, stirring speed, pH, and solution temperature. The maximum value for dye removal was about 98%. Adsorption data from the experimental work show that the results fit the PSO model. Also, the sorption mechanism for SPGMA was studied for different dye concentrations.[132]

The adsorption performance of a packed bed column with amine-functionalized radiation-induced grafted fibers (AFF) for the removal of acid blue 80 (AB 80) was investigated.[133] GMA was grafted with banana fibers using electron beam irradiation and was subsequently functionalized with imidazole, which was used as the precursor for anionic dye adsorption. The effect of the flow rate, bed height, and inlet concentration on the breakthrough curves was analyzed in terms of the AFF adsorption performance. The experiment revealed that an increase in the bed height and inlet concentration promoted the adsorption efficacy, whereas a reduction was observed when the flow rate was increased. The highest bed capacity obtained was 194.45 mg g^{-1}, at a flow rate of 5 mL min^{-1}, a 100 mg L^{-1} inlet concentration, and a bed height of 50 mm. To determine the optimum operational parameters, the data collected *via* the experiments were fitted to the Yoon–Nelson model, the Thomas model and the bed depth service time (BDST) mathematical model. Under various conditions, the Thomas model closely defined the behavior of the breakthrough curves. The maximum adsorption capacity calculated from Yoon–Nelson and Thomas models increased with the increase in flow rate and inlet concentration. However, a reduction was observed with the increase in bed height. Fig. 16 displays the FE-SEM cross-sectional views for the GMA grafted fibers, AFF, and dye-loaded fibers. The micrographs clearly illustrate hollow-centered banana trunk fibers with a decrease in the diameter after functionalization and the dye-adsorption process.[133]

Metin[134] prepared a polyGMA–zeolite (PGMA–Z) composite *via* free radical polymerization, which was further modified to contain amino groups on its surface by reaction with hexamethylenediamine (HMDA) (PGMA–Z–HMDA). FT-IR, TGA, and SEM analyses were performed and investigated its potential as an adsorbent for the removal of anionic dyes reactive red 120 (RR120) and reactive blue 4 (RB4). The effect of the operational parameters was investigated. Maximum RR120 and RB4 adsorption capacities of the composite were calculated as 136.5 and 189.8 mg g^{-1}, respectively. Isotherm, kinetics, and thermodynamics studies were also performed. It was found that the adsorption process might be heterogeneous by nature, and the adsorption kinetics of these reactive dyes followed the PSO. The thermodynamics calculations showed that the adsorption process was spontaneous and exothermic. To determine the surface morphology and surface characteristics, the SEM images of natural zeolite and PGMA–Z–HMDA particles were evaluated and are shown in Fig. 17. Selected SEM images of natural zeolite indicated that it has an irregular and layered structure (Fig. 17A). The morphological appearance of the PGMA–Z–HMDA composite was evaluated under different magnitudes. As shown in Fig. 17B, the PGMA particles are located on Z layers. From Fig. 17B, we can also say that the morphological appearance of the polymer shows a globular form, where these particles interconnected and formed aggregates.[134]

The removal of MB from aqueous solutions has been carried out using synthesized orthophosphoric acid-doped pyrazole-*g*-PGMA (OPA-Py-*g*-PGMA) and PGMA particles of average size 71 and 40 μm, respectively, conducted under batch conditions.[135] The kinetic and equilibrium results obtained for MB sorption with different initial MB concentrations onto synthesized OPA-Py-*g*-PGMA, and PGMA were analyzed. The analysis of the kinetic data indicated that the sorption was a second-order process. An ion-exchange mechanism may have existed in the MB-sorption

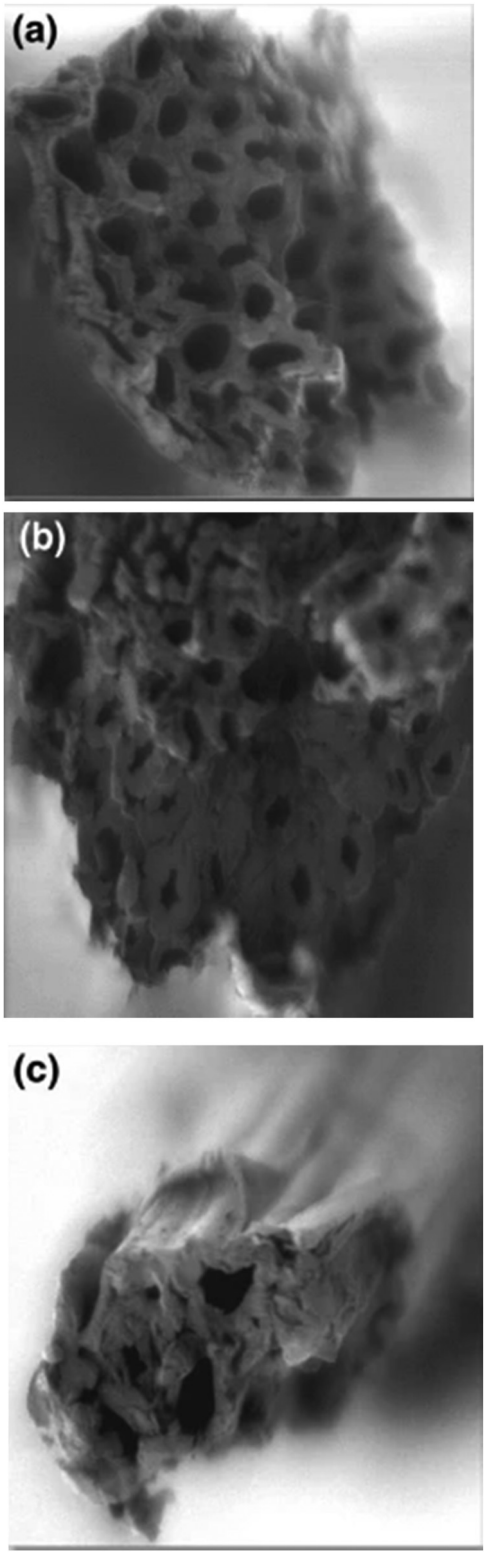

Fig. 16 FE-SEM cross-sectional images of hollow-centered banana trunk fiber for (a) GMA grafted fibers, (b) AFF, and (c) dye-loaded fibers with a magnification of ×500.[133] Reproduced from ref. 133, with permission from Springer Nature, 2019.

process with the synthesized OPA-Py-*g*-PGMA. The MB uptake by OPA-Py-*g*-PGMA and PGMA was quantitatively evaluated using

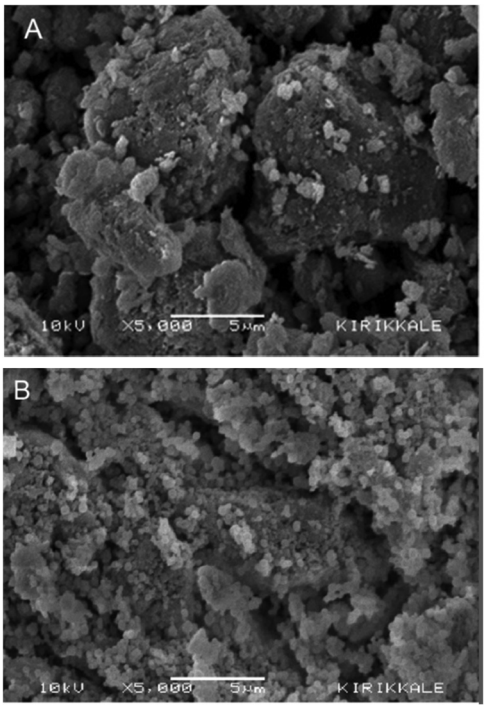

Fig. 17 SEM micrographs of different parts of samples at 5000× magnification. (A) natural zeolite, and (B) PGMA–Z–HMDA composite.[134] Reproduced from ref. 134, with permission from John Wiley and Sons, 2016.

equilibrium sorption isotherms. To describe the isotherms mathematically, the experimental data of the removal equilibrium correlated with the Langmuir, Freundlich, Temkin, and Dubinin–Radushkevich (D–R) isotherm models, and the applicability of these isotherm equations to the sorption systems was compared *via* the correlation coefficients. The maximum sorption capacities, determined from the Langmuir isotherm, were 15.15 and 8.67 mg g^{-1} at 25 °C for OPA-Py-*g*-PGMA and PGMA, respectively. Moreover, the diffusion mechanism of MB was described using different adsorption diffusion models. The diffusion rate equations of Dumwald–Wagner and intraparticle models were used to calculate the diffusion rate. The actual rate-controlling step involved in the MB sorption process was determined by further analysis of the sorption data by the kinetic expression given by Boyd.[135]

Poly(HEMA-*co*-MMA) beads were prepared from (2-hydroxyethyl methacrylate) (HEMA) and methyl methacrylate (MMA) in the presence of $FeCl_3$.[136] Thermal co-precipitation of Fe(III) ions containing beads with Fe(II) ions was carried out under alkaline conditions. The magnetic beads were grafted with PGMA, and the epoxy groups of the grafted PGMA brushes were converted into amino groups through reaction with ammonia. The magnetic beads were characterized *via* surface area measurements, electron spin resonance (ESR), Mössbauer spectroscopy, and SEM. The maximum adsorption of the reactive green 19 (RG19) dye on the PGMA-grafted and amine-modified magnetic beads was around pH 3. The adsorption capacity of the magnetic beads was 84.6 mg g^{-1}. Batch kinetic sorption experiments showed that a PSO rate kinetic model was applicable. The PGMA-grafted and amine-modified magnetic beads (adsorbent) were expected to

have the advantage of the mobility of the grafted chains in the removal of acidic dyes from aqueous solutions. The magnetic beads show potential as an adsorbent for the removal of pollutants under various experimental conditions without any significant reduction in their initial adsorption capacity.[136]

A mutual radiation grafting technique using Co-60 gamma radiation has been used to graft GMA to Teflon scrap (TS).[137] Cationic and anionic adsorbents were prepared from GMA-*g*-TS by converting the epoxy ring into sulphonic acid and triamine groups *via* suitable chemical reactions at elevated temperatures. The converted grafted product was studied for its dye-uptake properties from manufactured aqueous dye solutions. The uptake of basic red 29 (BR29) and Remazol brilliant blue 1 (RBB1) was investigated. The equilibrium adsorption of BR29 and RBB1 was better explained using the Langmuir adsorption model. A higher coefficient of determination and a better agreement were obtained for the PSO kinetic model. A results of SEM shown in Fig. 18 clearly showed that, although Teflon is a highly crystalline polymer, prominent defects are visible in its core. It seems that the grafting of GMA takes place predominantly on the surfaces of these defects as they become more prominent and projected out of the matrix in the grafted matrix. Upon chemical treatment, the sample converted to sulphonic acid groups showed larger ordered domains than those of the amine-converted matrix. The shape and size of the domains would depend on the conversion method and the final drying procedure of the converted samples before recording of the SEM micrographs.[137]

Arica *et al.*[138] prepared magnetic MCM-41 (mMCM-41) composite particles and modified them with (3-aminopropyltriethoxysilane) (APTES), which were then grafted with PGMA *via* surface-initiated atom transfer radical polymerization (SI-ATRP). The PGMA-grafted magnetic MCM-41 particles were functionalized with (tris-2-aminoethylamine) (TAEA) and used as a cationic adsorbent for the adsorptive removal of direct blue 6 (DB6) and direct black 38 (DB38) from an aqueous medium.

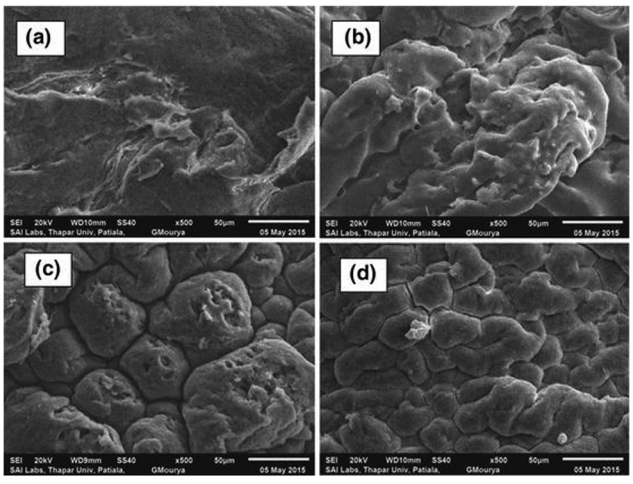

Fig. 18 SEM of (a) pristine TS, (b) grafted-TS (% grafting, 51.8%), (c) sulphonic acid grafted-TS (% conversion, 15.9%), and (d) aminated grafted-TS (% conversion, 16.2%).[137] Reproduced from ref. 137, with permission from Springer Nature, 2016.

The mMCM-41 and mMCM-41–PGMA–TAEA particles were characterized using BET, XRD, TGA, FT-IR, zeta potential, nitrogen adsorption–desorption isotherms (BET method), SEM, and analytical methods. VSM data showed that mMCM-41–PGMA–TAEA displays paramagnetic behavior with a saturation magnetization of about 19.6 emu g^{-1}. The adsorption potential of two different textile dyes DB-6 and DB-38 was evaluated by varying the experimental pH conditions, temperature, ionic strength, and initial dye concentration. Both dyes were removed from an aqueous medium with high efficiency over a wide range of pH 4–7. The equilibrium adsorption data were analyzed using Langmuir and Freundlich models. The experimental equilibrium data were found to fit the Langmuir model well for adsorption of the DB6 and DB38 dyes on the mMCM-41-*g*-PGMA–TAEA particles. It was found that the PSO model can describe the adsorption data well. The presented adsorbent can be regenerated using 0.1 M HNO_3 solution and the desorption efficiency was more than 96%. Hence, the mMCM-41 composite particles were very stable, and are easily regenerated.[138]

Arslan[139] removed methylene blue (MB) from aqueous solutions *via* a batch equilibration technique using a novel fibrous adsorbent that grafts the GMA and methacrylic acid (MAA) monomer mixture onto poly(ethylene terephthalate) (PET) fibers. The operational parameters investigated included the pH of the solution, the removal time, graft yield, dye concentration, and reaction temperature. The adsorption rate of MB was much higher on the MAA–GMA-*g*-PET fibers than on the ungrafted PET fibers. 99% of MB was removed for an initial dye concentration of 10 mg L^{-1}, and 93% was removed at 200 mg L^{-1} by the monomer-mixture-grafted PET fibers. It was found that the PSO kinetics equation described the dye-adsorption data on this fibrous adsorbent very well. The experimental isotherm data were analyzed using Langmuir and Freundlich isotherm models. The data showed that the Freundlich isotherm model fitted the data very well for the dyes on the adsorbent fibers. The adsorbed dye was easily desorbed *via* treatment with an acetic acid–methanol mixture (50% V/V) at room temperature. SEM images of the MAA–GMA-*g*-PET fibers (115%) are shown in Fig. 19. It is clear from the SEM results that the ungrafted PET fiber surface in Fig. 19a has a smooth and relatively homogeneous appearance. The grafted side chain GMA seems to form microphages attached to the PET backbone and causes a heterogeneous appearance in the graft copolymer in Fig. 19b, showing proof of grafting.[139]

The poly(hydroxymethyl methacrylate-*co*-GMA) (p(HEMA–GMA)) macroporous cryogel with a high density of epoxy groups was synthesized,[140] and the epoxy groups of the cryogel were modified into phosphonate groups. The effects of the dye concentration, adsorption time, pH, salt concentration, and adsorption temperature on the adsorption of direct blue 53 (DB53) and reactive blue 160 (RB160) dyes were studied. The maximum adsorption capacity was found to be 245.3 and 155.8 mg g^{-1} for the DB53 and RB160 dyes, respectively. The higher adsorption capacity achieved for the DB53 compared with the RB160 dye is a result of the pendant primary amino groups of the DB53 dye as well as the smaller size of the dye molecule. The Langmuir isotherm model and the PSO kinetic

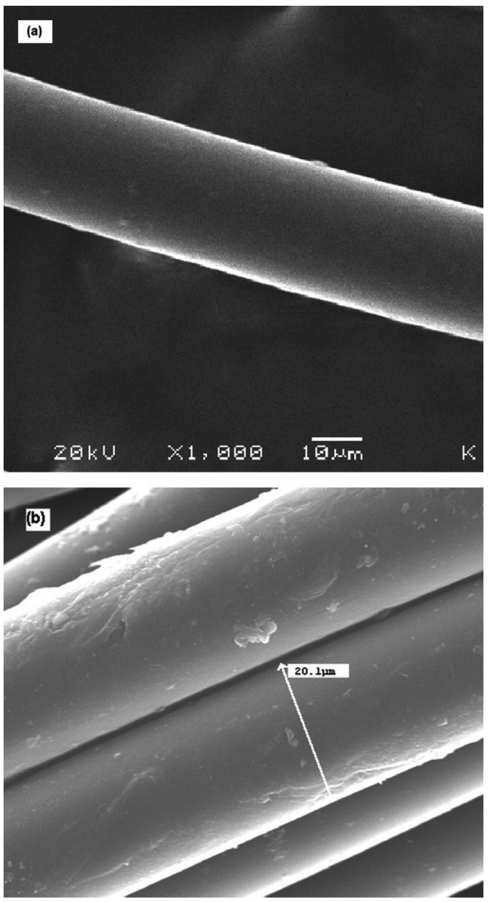

Fig. 19 (a) SEM micrograph of ungrafted PET fibers, and (b) SEM micrograph of MAA–GMA-grafted PET fibers (115%, 50/50 mol).[139] Reproduced from ref. 139, with permission from John Wiley and Sons, 2011.

model described the experimental data well. The p(HEMA–GMA)–PO_4^{2-} adsorbent has many operational advantages for the removal of pollutants. It could be a promising adsorbent for use in industrial WW treatment. The surface morphology of p(HEMA–GMA) and p(HEMA–GMA)–PO_4^{2-} was observed *via* SEM, as shown in Fig. 20(a and b), respectively. The surface of the cryogels has a sponge-like macroporous structure. The pores are irregular, and the radii of the interconnected pores are between 2 and 80 μm. These large pore sizes could provide an easy fluid mechanism for contacting the adsorptive sites of the cationic cryogel films for the dye molecule within the adsorption medium. Thus, the dye molecules within the solution can easily move through the pores without any diffusional restriction. It should be noted that after reacting with H_3PO_4, the surface morphology of the modified cryogel compared with the pristine counterpart did not change significantly.[140]

8. Comparison of different glycidyl methacrylate derivatives in dye removal

Table 6 compares the different GMA modifications in dye removal and shows the differences in pH, temperature, adsorption

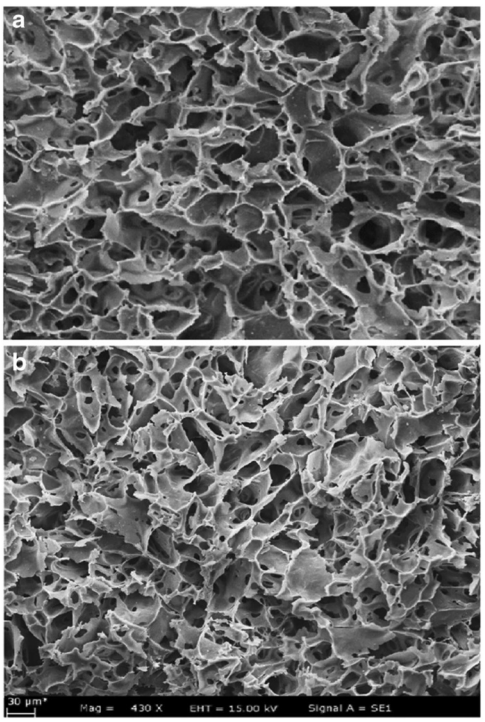

Fig. 20 SEM micrographs of the macroporous structure for (a) p(HEMA–GMA) and (b) p(HEMA–GMA)–PO_4^{2-}.[140] Reproduced from ref. 140, with permission from Springer Nature, 2020.

capacity, nature of the adsorption, dyes, and kinetic models and isotherms.

9. Bibliometric analysis of anionic dye removal by GMA

The subject "Anionic dye removal by glycidyl methacrylate" was used to search the Web of Science (WOS) database for publications on CS (retrieved on 20/02/2022). The study was conducted for the period of 2012 to 2022. During the timeframe of 2012–2022, a total of 17 publications was collected from WOS. The categories of chemistry multidisciplinary, polymer science, biochemistry molecular biology, chemistry applied, engineering chemical, and materials science textiles accounted for 41.18%, 35.29%, 11.77%, 11.77%, 11.77%, and 11.77%, of all 17 GMA publications, respectively (Table 7). From 2012 until 2018, GMA publications were rare. Since 2018, there has been an increase in the number of papers. With 5 papers, the year 2019 was the most productive, followed by 2016 and 2018, 2020, and 2021 with 4 and 2 papers, for the last three years respectively (Fig. 21). In terms of countries with GMA publications, People R CHINA had the most 4 out of 17 : 23.52%, followed by TURKEY 4 : 23.52%, and INDIA 3 : 17.64%. Egypt published 2 : 11.765%, followed by MALAYSIA with 2 : 11.765% (Fig. 22).

9. Future research recommendations

Recent advances in various CS compounds and GMA, as well as various methods for removing dyes and heavy metals from WW,

Table 6 Comparison of different GMA modifications in dye removal

Adsorbent	Dyes	pH	Temp. (°C)	Nature of adsorption	Adsorption capacity (mg g^{-1})	Kinetic model	Isotherm	References
Poly(ethylene terephthalate) copolymers grafted with GMA	Congo red, acid violet 7	3–5	25	—	98, 121	—	—	123
GMA cross-linked CS cryogels	Reactive yellow B-4RFN	—	—	—	224.6	PSO	Dubinin–Radushkevich	48
Dimethyl-aminoethyl methacrylate employing GMA-modified phytic acid as a cross-linker	Reactive red 24	3	30	—	1871.23	PSO	Langmuir	141
Cellulose nanocrystal-modified poly(2-hydroxyethyl methacrylate)–GMA	Methyl orange	6	—	—	455	PSO	Langmuir	128
PolyGMA–Fe_3O_4–diazoresin magnetic microspheres	Rhodamine B, methyl orange, methylene blue	5–13	—	—	—	—	—	142
PolyGMA–zeolite	Reactive red 120, reactive blue 4	2	25	Exothermic	136.5, 189.8	PSO	Langmuir, Freundlich	134
Magnetite core and GMA–*N*,*N*′-methylenebisacrylamide shell grafted diethylenetriamine	Acid yellow 99	3	25	Endothermic	128.6	PSO	Langmuir	125
Banana fiber-grafted GMA	Acid blue 80	—	—	—	—	—	Yoon–Nelson, Thomas	133
Pre-treated banana fibers grafted GMA	Acid blue 80, acid red 86	—	70	Exothermic	—	PSO	Langmuir, Freundlich	143
Divinylbenzene copolymer with GMA functionalized with triethylenetetramine	Acid green 16, acid violet 1, acid red 18	—	25	—	142.4, 172, 216.3	—	Freundlich	129
GMA-substituted dextran with acrylic acid	Methylene blue, crystal violet	6.6	20	Exothermic	1994, 2390	PSO	Langmuir, Freundlich	144
GMA grafted to Teflon scrap	Remazol brilliant blue 1	—	65	Exothermic	59.62, 55.62	PSO	Langmuir	137
CS with GMA and magnetite	Remazol brilliant blue R	2	25	Endothermic	95.86	PSO	Langmuir	67

Table 7 Number of publications according to Web of Science categories (subjects)

Web of science categories	Record count	Percentage of 17 publications
Chemistry multidisciplinary	7	41.18
Polymer science	6	35.29
Biochemistry molecular biology	2	11.77
Chemistry applied	2	11.77
Engineering chemical	2	11.77
Materials science textiles	2	11.77
Chemistry organic	1	5.88
Engineering environmental	1	5.88
Materials science composite	1	5.88
Materials sciences multidisciplinary	1	5.88
Materials science paper wood	1	5.88
Multidisciplinary sciences	1	5.88

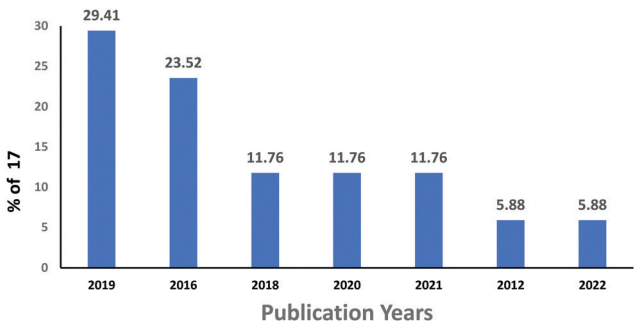

Fig. 21 Publications on anionic dye removal by GMA through the years.

have all been presented to provide a foundation for future research. This could be important for developing more effective contaminant-removal technologies and bridging the gap between laboratory and industry outcomes. In the future, improved CS- and GMA-based materials should be developed by combining them with additional bio or nanoscale reinforcements with excellent adsorption effectiveness. For understanding and improving pollutant sorption potential, a molecular modeling for pollutant degradation on CS and GMA composites is required. Also Determination of the reusability potential of these newly designed CS and GMA based adsorbents and focusing on improving reusability to make the processes economically feasible. To minimize various types of industrial effluents, the performance of several feasible CS, GMA, and CS/GMA hybrid materials is expected to enhance the physical and chemical properties of the hybrid material and should be investigated, and the reactivity of the hybrid sorbent can be improved by grafting new functional groups such as different amines on the epoxy group of GMA. In the future, it is highly recommended that modern optimization technologies should be used to create the most efficient materials and processes. This will not only lower the cost of experiments but will also enable the development of better processes more quickly.

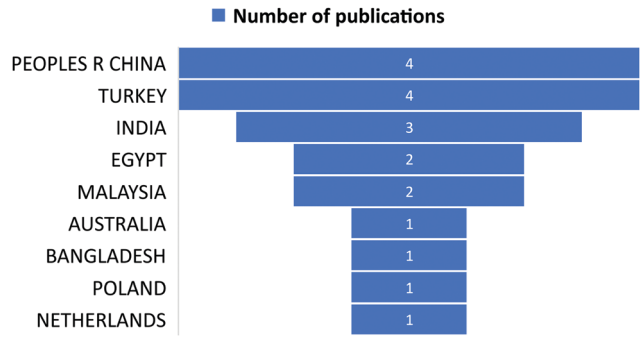

Fig. 22 Most countries published work the topic of anionic dye removal by GMA.

To mitigate hazardous pollutants, multifunctional materials based on CS and its modifications, as well as GMA, should be developed for the efficient removal of many types of industrially emitted pollutants.[26] Moreover, the authors strongly recommend studying the preparation of different CS, GMA, and their hybrid materials and studying their chemical and physical modifications for water treatment. Until now there have been very few studies on GMA, and CS hybrids.[145,146] Large surface areas, high pore volumes, and the presence of ligands and functional groups in the hybrid adsorbents make them efficient for different environmental applications. The adsorption potential of hybrids can be improved *via* surface treatment and functionalization. Efforts are being made to explore new adsorbents to design hybrid materials that target multi-pollutant removal. The use of these composites is a new and effective approach for the removal of toxic pollutants and dyes from aqueous solutions, although there remains a long way before on-site applications can be reached. In the future, hybrid adsorbents need to be proposed if we are to witness extensive applications on an industrial scale to minimize the menace of environmental pollution.

10. Conclusion

This Review presents a summary of pollution by heavy metals and organic dyes in the environment, with a focus on water, and reasons that its treatment using CS- or GMA-based sorbents is a cost-effective and environmentally friendly way to remove colors and heavy metals from WW. The sorbents could be modified using many physical and chemical methods to increase their surface area, functional groups, and sorption active sites. These adsorbents have undoubtedly displayed a remarkable efficiency in tackling various pollutants. There are several mechanisms of adsorption for the removal of both inorganic and organic compounds, of which electrostatic contacts, ion exchange, and complexation are the most mentioned. Due to the great progress in the creation of various sorbents, several issues remain to be addressed for these materials, such as their pH stability, sorption capacity, and durability, and these must be tackled in future developments.

Author contributions

Raed A. Mashabi: methodology, data curation, and writing original draft. Ziya A. Khan: methodology, investigation, data curation, review, and editing. Khalid Z. Elwakeel: methodology, data curation, review, and editing.

Conflicts of interest

The authors declare that they have no known competing financial interests or personal relationships that could have appeared to influence the work reported in this paper.

References

1 G. Sriram, A. Bendre, E. Mariappan, T. Altalhi, M. Kigga, Y. C. Ching, H.-Y. Jung, B. Bhaduri and M. Kurkuri, *Sustainable Mater. Technol.*, 2022, **31**, e00378.
2 A. M. Elgarahy, K. Z. Elwakeel, S. H. Mohammad and G. A. Elshoubaky, *Cleaner Eng. Technol.*, 2021, **4**, 100209.
3 P. Sirajudheen, N. C. Poovathumkuzhi, S. Vigneshwaran, B. M. Chelaveettil and S. Meenakshi, *Carbohydr. Polym.*, 2021, **273**, 118604.
4 N. Benit and A. S. J. I. J. o I. S. Roslin, *Eng. Technol.*, 2015, **2**, 691–696.
5 P. Sirajudheen and S. Meenakshi, *Int. J. Biol. Macromol.*, 2019, **133**, 253–261.
6 S. Natarajan, H. C. Bajaj and R. J. Tayade, *J. Environ. Sci.*, 2018, **65**, 201–222.
7 A. Azari, M. Noorisepehr, E. Dehghanifard, K. Karimyan, S. Y. Hashemi, E. M. Kalhori, R. Norouzi, S. Agarwal and V. K. Gupta, *Int. J. Biol. Macromol.*, 2019, **131**, 633–645.
8 G. Tchobanoglous, F. L. Burton and H. D. Stensel, *Wastewater engineering treatment and reuse*, McGraw-Hill Higher Education, Boston, US, 2003.
9 F. Hou, D. Wang, X. Ma, L. Fan, T. Ding, X. Ye and D. Liu, *Ultrason. Sonochem.*, 2021, **70**, 105327.
10 K. Z. Elwakeel, *J. Dispersion Sci. Technol.*, 2010, **31**, 273–288.
11 A. Reizabal, C. M. Costa, P. G. Saiz, B. Gonzalez, L. Pérez-Álvarez, R. Fernández de Luis, A. Garcia, J. L. Vilas-Vilela and S. Lanceros-Méndez, *J. Hazard. Mater.*, 2021, **403**, 123675.
12 S.-J. Chao, K.-H. Chung, Y.-F. Lai, Y.-K. Lai and S.-H. Chang, *Int. J. Biol. Macromol.*, 2021, **173**, 211–218.
13 L. Chen, Y. Zhu, Y. Cui, R. Dai, Z. Shan and H. Chen, *Chem. Eng. J.*, 2021, **405**, 126953.
14 O. Bozkaya, K. Günay, M. Arslan and Z. Gün Gök, *Res. Chem. Intermed.*, 2021, **47**, 2075–2093.
15 Z. Zhou, J. Sun and W. Zhou, *IOP Conf. Ser. Earth Environ. Sci.*, 2021, **639**, 012032.
16 M. Pasichnyk, M. Václavíková and I. Melnyk, *J. Polym. Res.*, 2021, **28**, 56.
17 K. Z. Elwakeel and M. Rekaby, *J. Hazard. Mater.*, 2011, **188**, 10–18.
18 N. Suryawanshi and J. S. Eswari, *Biomass Convers. Biorefin.*, 2022, **12**, 1977–1984.

19 M. S. Almughamisi, Z. A. Khan, W. Alshitari and K. Z. Elwakeel, *J. Polym. Environ.*, 2020, **28**, 47–60.
20 K. Z. Elwakeel, A. S. Al-Bogami and A. M. Elgarahy, *J. Polym. Environ.*, 2018, **26**, 2018–2029.
21 A. Rył and P. Owczarz, *Carbohydr. Polym.*, 2021, **255**, 117377.
22 E. Melro, F. E. Antunes, G. J. da Silva, I. Cruz, P. E. Ramos, F. Carvalho and L. Alves, *Polymers*, 2021, **13**, 1.
23 A. Irastorza, I. Zarandona, M. Andonegi, P. Guerrero and K. d l Caba, *Food Hydrocolloids*, 2021, 106633, DOI: 10.1016/j.foodhyd.2021.106633,.
24 S. Torkaman, H. Rahmani, A. Ashori and S. H. M. Najafi, *Carbohydr. Polym.*, 2021, **258**, 117675.
25 G. Cavallaro, S. Micciulla, L. Chiappisi and G. Lazzara, *J. Mater. Chem. B*, 2021, **9**, 594–611.
26 S. A. Qamar, M. Ashiq, M. Jahangeer, A. Riasat and M. Bilal, *Case Stud. Chem. Environ. Eng.*, 2020, **2**, 100021.
27 T. Winie and N. S. Mohd Shahril, *Front. Mater. Sci.*, 2015, **9**, 132–140.
28 A. Kausar, *Polym.-Plast. Technol. Mater.*, 2019, **58**, 934–947.
29 T. S. Anirudhan, L. Divya and J. Parvathy, *J. Chem. Technol. Biotechnol.*, 2013, **88**, 878–886.
30 A. A. Galhoum, W. H. Eisa, I. El-Tantawy El-Sayed, A. A. Tolba, Z. M. Shalaby, S. I. Mohamady, S. S. Muhammad, S. S. Hussien, T. Akashi and E. Guibal, *Environ. Pollut.*, 2020, **264**, 114797.
31 R. V. Kandisa, K. N. Saibaba, K. B. Shaik and R. Gopinath, *J. Biorem. Biodegrad.*, 2016, **7**, 371.
32 S. Khamparia and D. Jaspal, in *Handbook of Environmental Materials Management*, ed. C. M. Hussain, Springer International Publishing, Cham, 2018, pp. 1–14, DOI: 10.1007/978-3-319-58538-3_8-1.
33 M. Eumann and C. Schaeberle, in *Brewing Materials and Processes*, ed. C. W. Bamforth, Academic Press, San Diego, 2016, pp. 97–111, DOI: 10.1016/B978-0-12-799954-8.00005-8.
34 N. Al-Bastaki, *Chem. Eng. Process.*, 2004, **43**, 1561–1567.
35 D. M. Lewis, *Color. Technol.*, 2014, **130**, 382–412.
36 M. Sun, J. Ma, M. Zhang, Y. Xiao, Y. Zhu and S. Zhang, *Mater. Chem. Phys.*, 2020, **241**, 122450.
37 Z. Jia, S. X. Liang, W. C. Zhang, W. M. Wang, C. Yang and L. C. Zhang, *J. Taiwan Inst. Chem. Eng.*, 2017, **71**, 128–136.
38 Z. Yang, W. Shen, Q. Chen and W. Wang, *Dyes Pigm.*, 2021, **184**, 108835.
39 Ö. Açışlı, İ. Acar and A. Khataee, *Chemosphere*, 2022, **295**, 133870.
40 A. Szyguła, E. Guibal, M. A. Palacín, M. Ruiz and A. M. Sastre, *J. Environ. Manage.*, 2009, **90**, 2979–2986.
41 M. Ghalkhani, N. Zare, F. Karimi, C. Karaman, M. Alizadeh and Y. Vasseghian, *Food Chem. Toxicol.*, 2022, **161**, 112830.
42 Q. Liu, N. Xia, W. Wan, Y. Gao and S. Zhu, *Int. J. Biol. Macromol.*, 2021, **189**, 722–733.
43 J. Zhao, H. Liu, P. Xue, S. Tian, S. Sun and X. Lv, *Carbohydr. Polym.*, 2021, **274**, 118664.
44 F. Jummaat, E. B. Yahya, A. Khalil H.P.S, A. S. Adnan, A. M. Alqadhi, C. K. Abdullah, A. Sofea A.K, N. G. Olaiya and M. Abdat, *Polymers*, 2021, **13**, 633.
45 J.-W. Rhim, H.-M. Park and C.-S. Ha, *Prog. Polym. Sci.*, 2013, **38**, 1629–1652.
46 T. Jóźwiak and U. Filipkowska, *Sci. Rep.*, 2021, **11**, 13382.
47 G. Z. Kyzas, D. N. Bikiaris and A. C. Mitropoulos, *Polym. Int.*, 2017, **66**, 1800–1811.
48 M. Yin, X. Li, Y. Liu and X. Ren, *Carbohydr. Polym.*, 2021, **266**, 118129.
49 M. A. Khapre and R. M. Jugade, *Chem. Afr.*, 2021, **4**, 993–1005.
50 K. Z. Elwakeel, *J. Hazard. Mater.*, 2009, **167**, 383–392.
51 F. Banisheykholeslami, M. Hosseini and G. Najafpour Darzi, *Int. J. Biol. Macromol.*, 2021, **177**, 306–316.
52 N. Ahmad, S. Sultana, S. M. Faisal, A. Ahmed, S. Sabir and M. Z. Khan, *RSC Adv.*, 2019, **9**, 41135–41150.
53 Y.-S. Chen, C. W. Ooi, P. L. Show, B. C. Hoe, W. S. Chai, C.-Y. Chiu, S. S. S. Wang and Y.-K. Chang, *Membranes*, 2022, **12**, 63.
54 J. Cui, X. Wang, S. Yu, C. Zhong, N. Wang and J. Meng, *Int. J. Biol. Macromol.*, 2020, **165**, 2805–2812.
55 Q. Kong, X. Wang, X. Zhao and T. Lou, *J. Cleaner Prod.*, 2022, **331**, 130017.
56 L. Feng, X. Li, W. Lu, Z. Liu, C. Xu, Y. Chen and H. Zheng, *Int. J. Biol. Macromol.*, 2020, **150**, 617–630.
57 T. Lu, Y. Zhu, Y. Qi, W. Wang and A. Wang, *Desalin. Water Treat.*, 2018, **118**, 314–325.
58 V. Singh, A. K. Sharma, D. N. Tripathi and R. Sanghi, *J. Hazard. Mater.*, 2009, **161**, 955–966.
59 L. Wang, J. Zhang and A. Wang, *Desalination*, 2011, **266**, 33–39.
60 X. Fang, H. Guo, F. Yang and X. Bai, *Chem. Res. Chin. Univ.*, 2015, **31**, 1051–1055.
61 H. Sehil, M. Badaoui and A. Chougui, *Polym. Sci., Ser. B*, 2021, **63**, 853–865.
62 S. R. Patel and M. P. Patel, *Polym. Bull.*, 2022, DOI: 10.1007/s00289-021-04017-w.
63 R. Kaveh and M. Bagherzadeh, *Diamond Relat. Mater.*, 2022, **124**, 108923.
64 C. Cao, L. Xiao, C. Chen, X. Shi, Q. Cao and L. Gao, *Powder Technol.*, 2014, **260**, 90–97.
65 F. Wang, L. Li, J. Iqbal, Z. Yang and Y. Du, *Int. J. Biol. Macromol.*, 2022, **199**, 234–242.
66 H. Zhang, R. Li and Z. Zhang, *Environ. Pollut.*, 2022, **293**, 118517.
67 K. Z. Elwakeel, A. A. El-Bindary, A. Ismail and A. M. Morshidy, *RSC Adv.*, 2016, **6**, 22395–22410.
68 K. Elwakeel, A. El-Bindary, A. Ismail and A. Morshidy, *J. Dispersion Sci. Technol.*, 2017, **38**, 943–952.
69 K. Z. Elwakeel, M. A. Abd El-Ghaffar, S. M. El-kousy and H. G. El-Shorbagy, *Chem. Eng. J.*, 2012, **203**, 458–468.
70 I. Alina, A. M. Celina, H. Doina, C. Ovidiu and P. M. Ionel, *Green Mater.*, 2018, **6**, 149–156.
71 S. Yu, J. Wang and J. Cui, *Int. J. Biol. Macromol.*, 2020, **156**, 1474–1482.
72 S. Yu, J. Cui, H. Jiang, C. Zhong and J. Meng, *Int. J. Biol. Macromol.*, 2019, **134**, 830–837.
73 S. Q. Hu, Y. H. Chen, K. Xie, X. Qi and T. R. Zhu, *Adv. Mater. Res.*, 2014, **864-867**, 659–663.

74 L. Zhang, L. Sellaoui, D. Franco, G. L. Dotto, A. Bajahzar, H. Belmabrouk, A. Bonilla-Petriciolet, M. L. S. Oliveira and Z. Li, *Chem. Eng. J.*, 2020, **382**, 122952.
75 X. Zhao, X. Wang and T. Lou, *Carbohydr. Polym.*, 2022, **276**, 118728.
76 M. S. Baburaj, C. T. Aravindakumar, S. Sreedhanya, A. P. Thomas and U. K. Aravind, *Desalination*, 2012, **288**, 72–79.
77 T. M. Masilompane, N. Chaukura, S. B. Mishra and A. K. Mishra, *Int. J. Biol. Macromol.*, 2018, **120**, 1659–1666.
78 A. Ü. Metin, H. Çiftçi and E. Alver, *Ind. Eng. Chem. Res.*, 2013, **52**, 10569–10581.
79 V. Nair, A. Panigrahy and R. Vinu, *Chem. Eng. J.*, 2014, **254**, 491–502.
80 W. Nitayaphat, *Mater. Today: Proc.*, 2017, **4**, 6274–6283.
81 Z. M. Şenol, N. Gürsoy, S. Şimşek, A. Özer and N. Karakuş, *Int. J. Biol. Macromol.*, 2020, **148**, 635–646.
82 V. Janaki, B.-T. Oh, K. Shanthi, K.-J. Lee, A. K. Ramasamy and S. Kamala-Kannan, *Synth. Met.*, 2012, **162**, 974–980.
83 H. Karaer and İ. Uzun, *Desalin. Water Treat.*, 2013, **51**, 2294–2305.
84 H. Q. Le and Y. Shimoyama, *J. Chem. Eng. Jpn.*, 2019, **52**, 671–679.
85 P. Banerjee, S. R. Barman, A. Mukhopadhayay and P. Das, *Chem. Eng. Res. Des.*, 2017, **117**, 43–56.
86 C. Qiu, Q. Tang, X. Zhang, M.-C. Li, X. Zhang, J. Xie, S. Zhang, Z. Su, J. Qi, H. Xiao, Y. Chen, Y. Jiang, C. F. de Hoop and X. Huang, *J. Cleaner Prod.*, 2022, **338**, 130550.
87 S. Ranjbari, A. Ayati, B. Tanhaei, A. Al-Othman and F. Karimi, *Environ. Res.*, 2022, **204**, 111961.
88 N. P. Raval, S. Mukherjee, N. K. Shah, P. Gikas and M. Kumar, *J. Environ. Manage.*, 2021, **280**, 111680.
89 A. Bayat, A. Tati, S. Ahmadipouya, S. A. Haddadi and M. Arjmand, *J. Mol. Liq.*, 2021, **331**, 115734.
90 H. Zhu, Y. Fu, R. Jiang, J. Yao, L. Liu, Y. Chen, L. Xiao and G. Zeng, *Appl. Surf. Sci.*, 2013, **285**, 865–873.
91 L. Obeid, A. Bée, D. Talbot, S. B. Jaafar, V. Dupuis, S. Abramson, V. Cabuil and M. Welschbillig, *J. Colloid Interface Sci.*, 2013, **410**, 52–58.
92 K. Z. Elwakeel, *J. Hazard. Mater.*, 2009, **167**, 383–392.
93 H. Yan, H. Li, H. Yang, A. Li and R. Cheng, *Chem. Eng. J.*, 2013, **223**, 402–411.
94 L. Fan, C. Luo, X. Li, F. Lu, H. Qiu and M. Sun, *J. Hazard. Mater.*, 2012, **215-216**, 272–279.
95 H. Jiang, P. Chen, S. Luo, X. Luo, X. Tu, Q. Cao, Y. Zhou and W. Zhang, *J. Inorg. Organomet. Polym. Mater.*, 2013, **23**, 393–400.
96 A. Debrassi, A. F. Corrêa, T. Baccarin, N. Nedelko, A. Ślawska-Waniewska, K. Sobczak, P. Dłużewski, J.-M. Greneche and C. A. Rodrigues, *Chem. Eng. J.*, 2012, **183**, 284–293.
97 S. H. Sanlier, G. Ak, H. Yilmaz, G. Ozbakir and O. Cagliyan, *Prep. Biochem. Biotechnol.*, 2013, **43**, 163–176.
98 H.-Y. Zhu, R. Jiang, L. Xiao and W. Li, *J. Hazard. Mater.*, 2010, **179**, 251–257.
99 N. A. Travlou, G. Z. Kyzas, N. K. Lazaridis and E. A. Deliyanni, *Langmuir*, 2013, **29**, 1657–1668.
100 L. Fan, C. Luo, M. Sun, H. Qiu and X. Li, *Colloids Surf., B*, 2013, **103**, 601–607.
101 H. Y. Zhu, Y. Q. Fu, R. Jiang, J. Yao, L. Xiao and G. M. Zeng, *Bioresour. Technol.*, 2012, **105**, 24–30.
102 H. Zhu, M. Zhang, Y. Liu, L. Zhang and R. Han, *Desalin. Water Treat.*, 2012, **37**, 46–54.
103 H. Y. Zhu, R. Jiang, L. Xiao and G. M. Zeng, *Bioresour. Technol.*, 2010, **101**, 5063–5069.
104 R. Jiang, Y.-Q. Fu, H.-Y. Zhu, J. Yao and L. Xiao, *J. Appl. Polym. Sci.*, 2012, **125**, E540–E549.
105 A. Debrassi, T. Baccarin, C. A. Demarchi, N. Nedelko, A. Ślawska-Waniewska, P. Dłużewski, M. Bilska and C. A. Rodrigues, *Environ. Sci. Pollut. Res.*, 2012, **19**, 1594–1604.
106 H. Y. Zhu, R. Jiang, Y. Q. Fu, J. H. Jiang, L. Xiao and G. M. Zeng, *Appl. Surf. Sci.*, 2011, **258**, 1337–1344.
107 L. Fan, Y. Zhang, C. Luo, F. Lu, H. Qiu and M. Sun, *Int. J. Biol. Macromol.*, 2012, **50**, 444–450.
108 Y.-C. Chang and D.-H. Chen, *Macromol. Biosci.*, 2005, **5**, 254–261.
109 N. A. Kalkan, S. Aksoy, E. A. Aksoy and N. Hasirci, *J. Appl. Polym. Sci.*, 2012, **124**, 576–584.
110 L. Fan, Y. Zhang, X. Li, C. Luo, F. Lu and H. Qiu, *Colloids Surf., B*, 2012, **91**, 250–257.
111 X. Xu, J. Yu, C. Liu, G. Yang, L. Shi and X. Zhuang, *React. Funct. Polym.*, 2021, **160**, 104840.
112 R. Chanajaree, M. Sriuttha, V. S. Lee and K. Wittayanarakul, *J. Mol. Liq.*, 2021, **322**, 114507.
113 F. Bahalkeh, M. Habibi juybari, R. Zafar Mehrabian and M. Ebadi, *Int. J. Biol. Macromol.*, 2020, **164**, 818–825.
114 X. Zhao, X. Wang and T. Lou, *J. Hazard. Mater.*, 2021, **403**, 124054.
115 F. Mashkoor and A. Nasar, *Int. J. Biol. Macromol.*, 2020, **161**, 88–100.
116 L. Zheng, C. Wang, Y. Shu, X. Yan and L. Li, *Colloids Surf., A*, 2015, **468**, 129–139.
117 M. Liu, Z. Xie, H. Ye, W. Li, W. Shi, Y. Liu and Y. Zhang, *Colloids Surf., A*, 2021, **627**, 127155.
118 B. Yuan, L.-G. Qiu, H.-Z. Su, C.-l Cao and J.-h Jiang, *Int. J. Biol. Macromol.*, 2016, **82**, 355–360.
119 S. Chatterjee, M. W. Lee and S. H. Woo, *Bioresour. Technol.*, 2010, **101**, 1800–1806.
120 A. ZabihiSahebi, S. Koushkbaghi, M. Pishnamazi, A. Askari, R. Khosravi and M. Irani, *Int. J. Biol. Macromol.*, 2019, **140**, 1296–1304.
121 M. H. Dehghani, A. Dehghan and A. Najafpoor, *J. Ind. Eng. Chem.*, 2017, **51**, 185–195.
122 I. A. Mohammed, A. H. Jawad, A. S. Abdulhameed and M. S. Mastuli, *Int. J. Biol. Macromol.*, 2020, **161**, 503–513.
123 O. Bozkaya, K. Günay, M. Arslan and Z. Gün Gök, *Res. Chem. Intermed.*, 2021, **47**, 2075–2093.
124 Z. P. Sandić, M. Žunić, D. Maksin, A. Milutinović Nikolić, A. R. Popović, D. M. Jovanović and A. Nastasović, *Hem. Ind.*, 2014, **68**, 685–699.
125 K. Z. Elwakeel, A. A. El-Bindary, A. Z. El-Sonbati and A. R. Hawas, *RSC Adv.*, 2016, **6**, 3350–3361.
126 A. E. Yayayuruk, *J. Environ. Prot. Ecol.*, 2018, **19**, 1738–1746.

127 A. I. Waly, M. A. Khedr, H. M. Ali and I. M. Ahmed, *Cleaner Eng. Technol.*, 2022, **6**, 100374.
128 K. Köse, M. Mavlan, M. Nuruddin, A. M. U. Gómez and J. P. Youngblood, *Cellulose*, 2022, **29**, 1623–1636.
129 M. Wawrzkiewicz, B. Podkościelna and P. Podkościelny, *Molecules*, 2020, **25**(22), 5247.
130 R. K. Sharma and R. Kumar, *Int. J. Biol. Macromol.*, 2019, **134**, 704–721.
131 Á. Kuki, L. Nagy, M. Zsuga and S. Kéki, *Int. J. Mass Spectrom.*, 2011, **303**, 225–228.
132 M. Abu-Saied and N. A. Taha, *Global NEST J.*, 2020, **22**, 179–184.
133 S. Selambakkannu, N. A. F. Othman, K. A. Bakar and Z. A. Karim, *SN Appl. Sci.*, 2019, **1**, 175.
134 A. U. Metin, *Polym. Compos.*, 2016, **37**, 2313–2322.
135 M. S. Mohy Eldin, K. M. Aly, Z. A. Khan, A. E. M. Mekky, T. S. Saleh and A. S. Al-Bogami, *Desalin. Water Treat.*, 2016, **57**, 27243–27258.
136 G. Bayramoglu, B. Altintas and M. Y. Arica, *J. Chem. Technol. Biotechnol.*, 2012, **87**, 705–713.
137 C. V. Chaudhari, J. P. Guin, K. A. Dubey, Y. K. Bhardwaj and L. Varshney, *Polym. Bull.*, 2016, **73**, 2907–2926.
138 T. A. Arica, E. Ayas and M. Y. Arica, *Microporous Mesoporous Mater.*, 2017, **243**, 164–175.
139 M. Arslan, *J. Appl. Polym. Sci.*, 2011, **119**, 3034–3042.
140 G. Bayramoglu and M. Y. Arica, *Environ. Sci. Pollut. Res.*, 2020, **27**, 43340–43358.
141 W. Liu, R. Hu, Y. Li, Y. Huang, Y. Wang, Z. Wei, E. Yu and X. Guo, *RSC Adv.*, 2020, **10**, 4232–4242.
142 B. Yu, B. Yang, G. Li and H. Cong, *J. Mater. Sci.*, 2018, **53**, 6471–6481.
143 S. Selambakkannu, N. A. F. Othman, K. A. Bakar, T. T. Ming, R. D. Segar and Z. A. Karim, *Fibers Polym.*, 2019, **20**, 2556–2569.
144 Z. Yuan, J. Wang, Y. Wang, Q. Liu, Y. Zhong, Y. Wang, L. Li, S. F. Lincoln and X. Guo, *RSC Adv.*, 2019, **9**, 21075–21085.
145 K. Z. Elwakeel, M. F. Hamza and E. Guibal, *Chem. Eng. J.*, 2021, **411**, 128553.
146 K. Z. Elwakeel and E. Guibal, *Chem. Eng. J.*, 2015, **281**, 345–359.